Politecnico di Torino

POLITECNICO DI TORINO

Master Degree Thesis in Electronic Engineering

Development of High Brightness Blue Laser Source for Additive Manufacturing

Supervisors
Prof. Guido Perrone

Candidate
Sabina Zaimovic

Academic Year 2022-2023

Acknowledgements

Abstract

Recent applications of Additive Manufacturing (AM) pose new challenges that are difficult to meet with the commonly used Infrared (IR) laser, but instead could be well addressed by blue lasers. Indeed, while high-power IR lasers have found extensive usage in materials processing, switching to blue lasers would improve the processing quality and efficiency of some materials that are finding increasing importance in industrial applications, such as copper, gold and aluminum, because of their higher absorption in the blue wavelengths than in the IR region. This also improves the energy consumption since blue laser diodes show an higher Wall Plug Efficiency (WPE) than IR fiber lasers.

Advances in both laser technology and additive manufacturing processes are expected to drive further expansion and enable the implementation of innovative applications. In particular, efficient processing of high reflective metals and high-tech polymers require a blue laser source capable of emitting some hundreds of watts. Today, state of the art in high power blue laser sources are multi-emitter diode modules that deliver some tens of watts; therefore, to meet the application requirements a plurality of these modules must be multiplexed.

The aim of the thesis is to design a blue laser source for a system prototype of a new concept of low-cost Additive Manufacturing (AM) machine specific for the manufacturing of small-volume parts using high-performance semi-crystalline engineering thermoplastic or difficult to laser process metals.

The use of high brightness Blue Laser (BL) source enables the development of a flexible laser based system, composed of lower power multi emitter which eases the replacement in case of failures (graceful degradation), lowering the ownership costs, increasing the energy efficiency, and improving the product quality.

Among the various beam multiplexing approaches, wavelength (or spectral) combination of multi- emitter modules has been studied and implemented. Efficient wavelength multiplexing requires beams with stable spectral emission but the emission of laser diodes is heavily influenced by temperature and driving current. This problem can be solved by wavelength stabilization. This can be obtained by building an external cavity using diffraction gratings. As a preliminary step an experimental setup has been built to prove the feasibility of stabilization at different wavelength and in different conditions, like continuous or pulsed emission. The measurement has been complemented with simulations conducted using a finite element analysis-based software.

Then, the spectral combination of the multi-emitter module was analyzed using OpticStudio, an optical design software capable of analyzing complex sources in optical systems.

The obtained experimental results that followed are consistent with predictions, validating the adoption of spectral multiplexing to combine modules without deterioration of beam quality. The compactness and interchangeability of such approach opens the way to a modular configuration scalable both in power and brightness.

Contents

List of Figures

List of Tables

Chapter 1

Introduction

1.1 Additive manufacturing

Additive manufacturing, especially laser additive manufacturing (LAM), is a novel manufacturing technique for material processing which owns advantages of rapid prototyping, customization, high material utilization, and the ability to form complicated structures. It has been accurately defined as a process of joining materials to make objects from 3D model data [4]. It consists of layer-by-layer forming according to geometric model generated from computer aided design (CAD) software that allows fabrication of complex, custom metal or alloy products which is almost impossible to achieve by a conventional processing (e. g. subtractive manufacturing methodologies, forging, casting); moreover AM technology minimizes lead time by reason of no need of traditional process tools and procedures resulting in less material waste without subsequent part assembly process. AM technologies are already exploited by many applications in the field of automotive, aerospace, architecture, biomedical, electronics industries, based on the fact that a variety of materials including metals, ceramics, polymers and composite materials can be processed.

According to the difference of heat sources, AM technology for metal can be roughly classified into three types: wire and arc additive manufacturing (WAAM), electron beam additive manufacturing (EBAM) and laser additive manufacturing (LAM). WAAM is mainly suitable for rapid prototyping of large size components, while EBAM and LAM are both applicable for small parts. LAM is the most promising AM technology for metal currently.

1.1.1 Market trends

Recent years have witnessed a rapid growth of the laser market. As reported in Figure 1.1 [5], the Global Laser Technology Market Size accounted for USD 11.579 Million and is estimated to achieve a market size of USD 24,171 Million by 2030 growing at a CAGR of 8.7% from 2022 to 2030 [6].

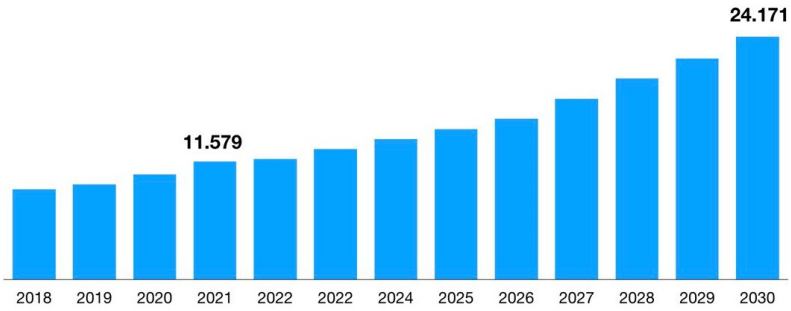

Figure 1.1: Global laser technology market revenue analysis and forecast.

By application, the laser processing segment has accounted 60% market share in 2021 as depicted in Figure 1.2.

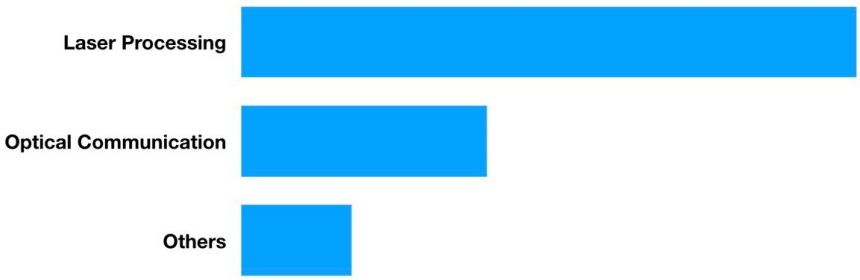

Figure 1.2: Global Laser Technology Market by application 2021 (USD Million).

Lasers have been the increasingly important core of additive manufacturing, with selective laser melting (SLM) becoming the fastest-growing Segment in the Metal Additive Manufacturing Market, as reported in Figure 1.3. SLM was valued at USD 1,395.20 million in 2017 and continued to grow until 2021. Due to the easy production of finite parts its demand is forecast to increase which, in turn, will boost the growth of the market during the next five years.

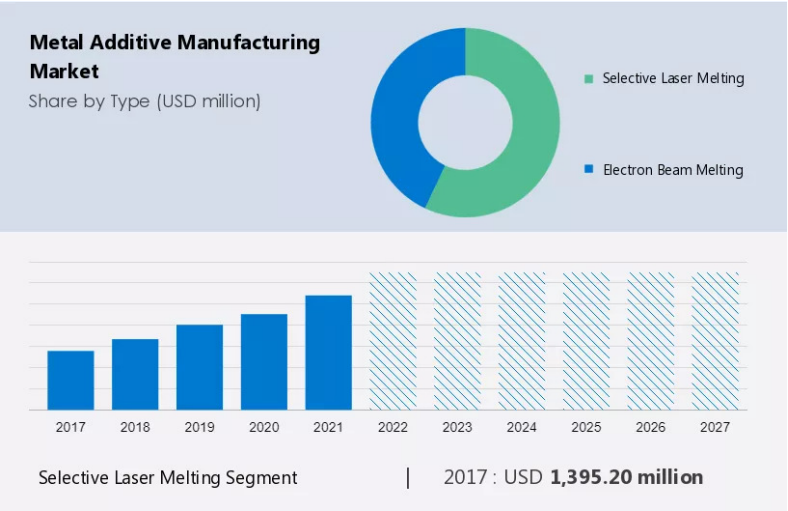

Figure 1.3: Metal Additive Manufacturing Market share by type.

In terms of laser type, Figure 1.4 shows that the solid-state laser segment will dominate the market during the forecast period due to the small region of the emission spectra used in the absorption process which leads to good absorption capability and great efficiency. Moreover, diode-pumped solid-state laser has the advantage of being extremely compact, light in weight and small in size.

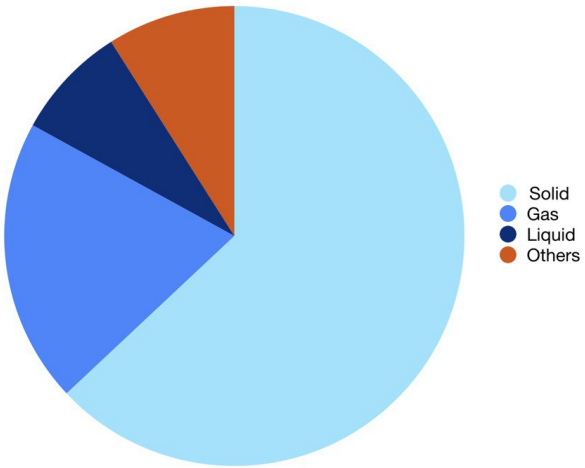

Figure 1.4: Global Laser Technology Market by laser type 2021 (% share).

1.2 Laser source

Carbon dioxide (CO2) lasers are one of the earliest gas discharge lasers and are the workhorse of precision manufacturing with 10.6 µm being the most widely used wavelength in AM. The disadvantages of this type of lasers are non-stable output power due to thermal expansion and contraction of the laser structure, their low Wall-Plug Efficiency (WPE) (5-15%) and their large size to guarantee air-tightness and dust-free operation. Moreover, optics with optimal mechanical properties at the working wavelength have poor availability.

As regards additive manufacturing, fiber lasers (FL) are one of the most widely used sources. A FL is a laser in which the active gain medium is a rare-earth doped optical fiber. The most suitable fiber dopant for high power generation is the Yb because of its high quantum efficiency (∼94%) and for this reason, Yb-fiber lasers are widely used in material processing and in particular are specifically employed in AM. This type of laser produces near-infrared output in 1030 nm-1080 nm range. As opposed to CO2, it shows off an higher WPE approximately between 30% and 40%. Furthermore, it has excellent beam quality, robustness against environmental disturbances, and system compactness.

For what concerns WPE in particular, Diode Lasers (DLs) are some of the most efficient devices in converting electrical into optical energy, working at wall plug efficiencies up to 50-80%. So far, High-power DLs are packaged in multi-emitter modules used for laser pumping of solid-state lasers among other applications. Although their beam quality is not as good as fiber lasers, DLs are increasingly used for direct material processing, as they have demonstrated improved performance in terms of more uniform melt and heating zones, greater consistency and repeatability compared to CO2 lasers. [7].

1.2.1 Laser parameters affecting AM

Lasers can be specified with several parameters such as average power, power stability, central wavelength, spectral bandwidth, beam diameter, beam quality, pulse energy, pulse duration and repetition rate.

The properties of the laser beam produced, included the wavelength of emission, depend on the gain medium and a particular range of wavelengths of choice could be convenient to process specific materials rather than others. The operating wavelength of the laser is the most important parameter to be considered in additive manufacturing because different materials interact with different laser wavelengths.

Figure 1.5 shows the absorptivity of various materials. In laser-based additive manufacturing, a high material absorption at the laser wavelength is desired since the target material should efficiently interact with the incident laser light; high absorptivity generally leads to high manufacturing throughput.

For metal powders, the shorter the wavelength, the better the light absorptivity,

therefore BLs is better absorbed than IR or CO2 lasers. The NIR laser is the current dominant laser, but the reflectivity of aluminum, copper and other non-ferrous metals at this wavelength are more than 95% leading to extremely poor energy utilization. In order to obtain a greater energy transfer, the NIR laser needs a higher output power. However, it is more likely to give rise to defects such as pores and cracks, and the forming quality of the workpiece is inferior. Therefore, overcoming the high laser reflectivity has become a key issue in laser metal processing. As reported in Figure 1.5 blue lasers is the best choice when dealing with metals due to the efficient absorption of those wavelength.

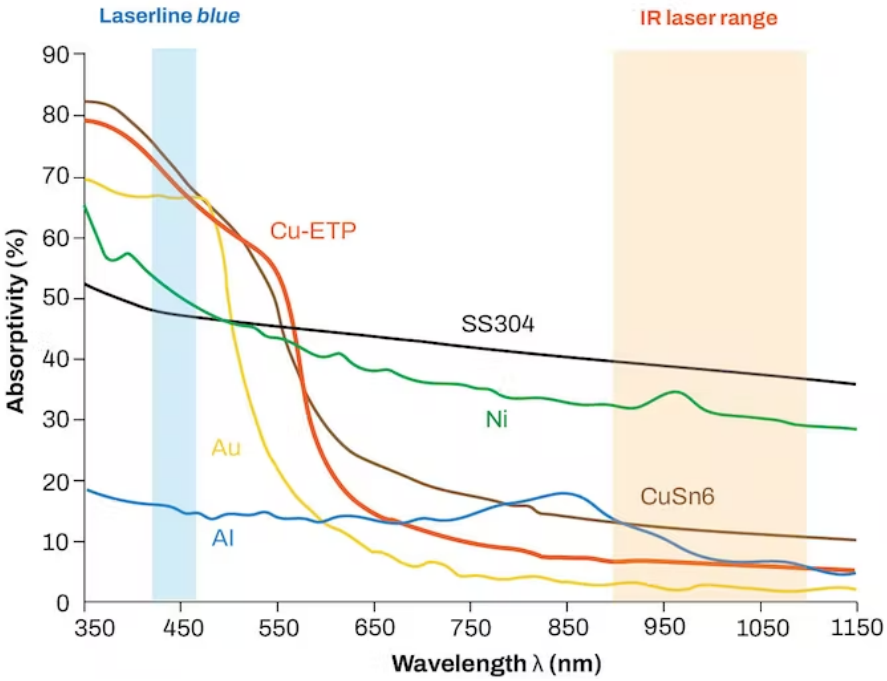

Figure 1.5: Absorption characteristics of various metals vs wavelength.

Moreover, blue laser heads feature much higher power density than CO2 and NIR lasers despite the lower total power. In fact, the state of the art for blue single emitter is 10 W, while IR single emitter can reach up to 30 W [8]. The reason behind the lower achievable power of GaN-based laser diode is the low power conversion efficiency (η_{PCE}). The most efficient laser diodes today are based on GaAs and some reach $\eta_{\mathrm{PCE}} > 70\%$ in continuous wave (CW) operation at room temperature while GaN-based laser diode can reach up to 40%. Large series resistance (one order of magnitude greater than GaAs-lasers'), increasing Auger recombination with high powers and enhanced free-carrier absorption are the main limiting factors [9].

At a given wavelength, beam quality and focused spot size are the laser parameters which should be considered to improve the manufacturing precision. To define beam

quality, Beam Parameter Product (BPP) is the product of the beam waist and the half-angle of beam divergence with the units of mm · mrad (millimeters times milliradians). Because the low BPP means Gaussian beam profile with higher energy confinement, BPP is closely correlated to the power density and affects the manufacturing resolution. The factor depends on the gain medium, pumping source, resonator structure, and operating wavelength. The latter, in particular, determines the lower limit of BPP, which is $\frac{\lambda}{\pi}$, defined as the diffraction-limit. The degree of variation of a laser beam from an ideal Gaussian one is represented by the M^2 factor.

As regards the injection of driving current in laser powder bed fusion process (L-PBF), CW or pulsed wave (PW) operation can be distinguished.
During the L-PBF, the metallic material undergoes a complex cycle of heating and cooling. Previous research has indicated that this thermal history can result in a range of issues with the deposited material, including defects such as lack of fusion and porosity, accumulation of residual stresses and microstructural inhomogeneity that can lead to anisotropy in the mechanical properties.
Melting and rapid solidification during the manufacturing process typically generate residual stresses, which can be reduced by preheating the build plate during manufacturing or by conducting post-thermal treatments such as stress relief and hot isostatic pressing.
An additional processing strategy to reduce these imperfections could be the use of PW.
There are several advantages to using pulsed lasers in additive manufacturing, as opposed to CW lasers.
Pulsed lasers can deliver much higher peak powers than CW lasers, which can be beneficial for tasks such as breaking up and removing material. This higher peak power can also lead to better material properties, such as increased density, smoother surface finish, and improved mechanical properties [10].
It also widens the range of materials that can be processed, including metals, ceramics, polymers, and composites overcoming the thermal conductivity of certain materials, allowing them to be melted and processed.
PW lasers provide increased control over the amount of heat being applied to the material, which can be important for preventing thermal damage to the workpiece and achieving optimal microstructural properties. In particular, Crystal structure of the as-built pulsed L-PBF material is less oriented and less columnar than continuous L-PBF resulting in stronger and stiffer pieces.
Moreover it can be used to achieve very fine feature sizes and high resolution, which is important for creating complex geometries and detailed structures.
The specific advantages will depend on the application and the specific properties of the material being processed. It has not been thoroughly examined and any work done to date has been focused on aluminium and titanium alloys. Hence, there is a gap in the state-of-the-art to see the effect of a pulsed laser heat source on the microstructure and mechanical properties of different materials and the possibility of achieving higher homogeneity in grain structure due to higher cooling rates.

1.3 Thesis Overview

Based on the introduced parameters in the previous section, a blue laser source has been designed for LAM and in particular for laser powder bed fusion of PEEK and metals.

The goal is to maximize the absorption in order to improve the efficiency avoiding imperfections due to excessive power density not properly absorbed by the powder. In order to do so, a blue laser system is been developed, aiming at reducing costs and providing a compact solution. Multi-emitters instead of fiber lasers have been selected to assure lower costs to detriment of beam quality. More in details the target for what concerns the spot size is set to 100 µm and the total power of the laser source settles down around 100 W.

The system developed consists of a unique block which incorporate the combined source and the processing head, mounted on an AM machine and relocated through a system of mechanical slides.

The source is modular, the building block is made of multi-emitters spectrally combined. The choice of such approach is motivated by the necessity to adapt the total power of the source to process different materials in order to minimize costs according to the number of modules used. In this way there is no need of reconfiguration of the entire system when there is necessity to scale power to process metals instead of plastic polymers. Coarse spectral combination is employed. In order to avoid overlapping of spectrum, an early step of stabilization is added to tune the emission at different wavelengths. The proposed scheme's only drawback is that the combined beam's emission spectrum contains the spectral contribution of the single emitters, resulting in decreased laser spectral brightness. However, for material processing applications, where spatial brightness is more important than spectral brightness, the proposed architecture has proven to be a valid alternative to other laser solutions.

For what concern the processing head, the presence of mechanical slides which move the source the use of a Galvo Mirror System is not fundamental and fixed optics have been preferred in order to contain costs.

In the present work, the focus is on the source and the power scaling technique adopted.
The preliminary laboratory tests have been performed on 30 W multi-emitter blue modules instead of the 60 W modules planned to be inserted in the final prototype. However, considering that the only difference between the 30 W and the 60 W modules is a polarization combination stage, the dimension of the spot is invariant and the CoC mounted, besides fabrication tolerances, share the same front reflection, thus the expected stabilized behaviour should be similar.
Thereafter effectiveness of stabilization has been tested with 444 nm VBG and not at the required wavelength for spectral combination due to unexpected component's delivery time. Results of stabilization are presented in chapter 3.
Finally, prototype structure spectral combination and ray tracing have been simulated

and presented in chapter 6 and chapter 5.

Chapter 2

Power Scaling Methods: an Overview

Key parameter for evaluating module performance is Radiance or Brightness. Given the optical power P, the M-squared value along x direction M_{x}^2, the M-squared value along the y direction M_{y}^2, a constant C that depends on the definition of beam size and divergence angles, it can be defined as:

$$B = \frac{CP}{\lambda^2(M_{\mathrm{x}}^2 M_{\mathrm{y}}^2)} \tag{2.1}$$

Equation 2.1 shows that Brightness is a measurement of both power and beam quality of a laser source. Moreover, radiance of an individual laser is conserved as its output propagates through any lossless optical system.

In the development of solid-state lasers, progress has been largely limited by thermooptic effects. To increase brightness, an increase of output power of the single-emitting device is needed through an increase of power density or an increase of active volume. However, if the power density on facets is increased, deterioration and damages of facets are more likely to happen, if the active volume is increased, the beam quality is reduced and distortion in the laser beam limits the diffraction-limited average power.
An alternative approach to develop high-power lasers is to use arrays of lower power lasers. Semiconductor and fiber gain elements are particularly attractive for beam-combined systems because of their high efficiency, the possibility to get near-diffraction-limited beams from the single elements, and they are easily built in array format. With recent advances in beam-combining technology, laser arrays are becoming an alternative for high-power, good-beam-quality laser system. Through the use of refractive, reflective or diffractive optical components, it is possible to increase the output power and/or improve brightness without or with minimal beam quality degradation.

Beams can be combined coherently or incoherently.
The propagation performance of coherent and incoherent beam combining has been studied in [11], and it has been found out that almost 4.5 times more energy will be encircled

in the coherent main-lobe compared with the incoherent combined beam when propagating in free-space. However, coherent combined beam is more sensitive and suffers more from different kinds of aberrations.

2.1 Coherent Beam Combining

In coherent combining (CBC), electric field are vectorally summed, thus multiple lasers are packaged into an array, in such a way to obtain constructive interference between all the elements. In order to do so, they must operates at the same wavelength and the relative phases must be kept under control within a small fraction of wavelength [12]. Figure 2.1 [13] provides a general schematic illustration of CBC which typically involve five principal parts: the geometry of splitting/combining, laser sources and amplifying section, phase-locking system, optical path difference (OPD) control, and number of channels.

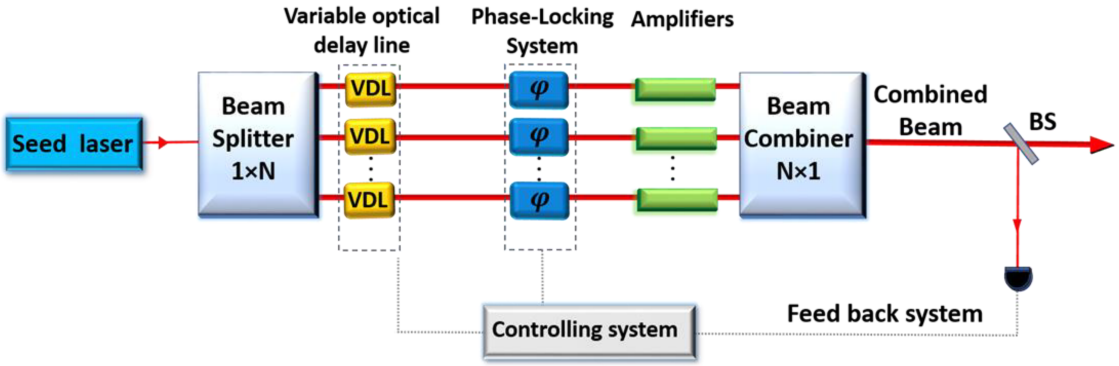

Figure 2.1: Schematic of coherent beam combining system.

The sophisticated phase controlling and the required single-frequency radiation are quite challenging and expensive at high power operations.
In coherent combining, the brightness scales as

$$B \propto f_{\mathrm{f}} N \tag{2.2}$$

where f_{f} is an efficiency factor less than or equal to 1 and N is the number of beams. If the emitting aperture grows proportional to N, than the on-axis intensity scales at N^2. If instead the aperture size is fixed then the on-axis intensity scales as N.
Even though Coherent beam combining narrows bandwidth and allows power and brightness to scale as the number of combined elements, it is never been used in commercial systems.

2.2 Incoherent Beam Combining

2.2.1 Spatial combination

Spatial combination, also known as Beam stacking or side-by-side combining, is an incoherent beam combining technique that exploits the superposition of chips arranged on one or more direction.
It is mainly used in multi-emitter module to increase the power coupled to the core of the delivery fiber and to compensate the divergence mismatch among the two main orthogonal directions. An example of multi-emitter realized with spatial beam combination is reported in Figure 2.2.

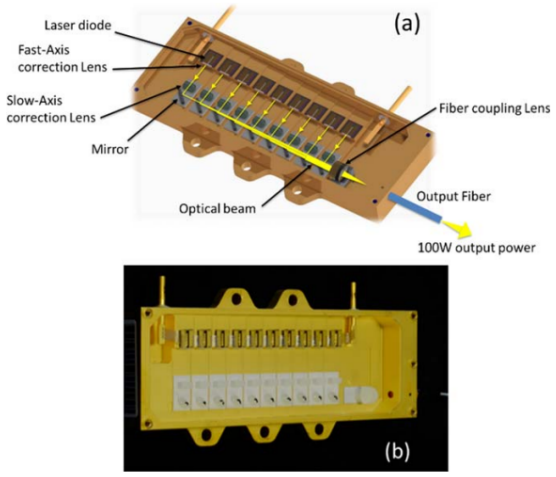

Figure 2.2: Multi-emitter schematic diagram (a) and picture of a fabricated module (b).

To improve divergence in slow axis (SA) direction in laser diode bar where chips are arranged along the SA, the beams must be rearranged along the fast axis (FA).
Beam Parameter Product (BPP) is the limiting factor of spatial combination since it limits the maximum number of beams that can be coupled to a fiber. BPP for Gaussian beams is defined as the product between the beam radius at the waist and the beam divergence half angle at far field.
Assuming that each beam has the same power, beam size and divergence, the divergence of stack will not change, but power and beam size tend to increase proportionally to the number of beams.

$$B = \frac{NP}{NA\theta} \tag{2.3}$$

As shown in Equation 2.3, where N is the number of beams combined, A is the area of each beam, brightness cannot be improved using spatial combination (brightness-theorem limited) and, therefore, this cannot be used to obtain near-diffraction-limited outputs from laser arrays. However, particular care should be used in selecting the optical component since they can cause a remarkable deterioration. As already introduced, higher the number of chips, higher the output power, but stacking to obtain high power

multi-emitters makes thermal management more difficult, influencing reliability. A better compromise seems to be combination of less powerful modules to obtain high power output thus relaxing thermal constrains and costs of replacement.

2.2.2 Polarization Beam Combining

To improve output power in multi-emitter polarization beam combining is adopted. It is usually performed as the last step inside modules to combine two linearly polarized laser beams as shown in Figure 2.3. It requires polarized input beams crossing a thin film polarizer and leads to an unpolarized output beams with twice the input optical power (except some parasitic losses), the same beam quality and a nearly doubled brightness.
As the polarization purity of the diode laser is typically 95% or less, this method results in some loss of power in exchange for increased optical real density. It can be employed only once.

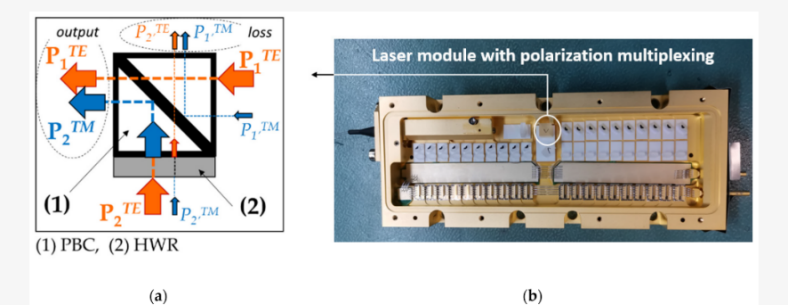

Figure 2.3: (a) Polarization multiplexing scheme of two laser beams P1 and P2 with a Polarization Beam Cube (PBC) and an Half Wave Rotator (HWR). Thick shaded lines and arrows represent the main beam components while thin shaded lines and arrows represent the minor components. TE polarization is shown in orange while TM polarization is shown in blue. (b) picture of the multi-emitter module fabricated based on PM of two laser beams obtained by two sets of the HPLD.

2.2.3 Spectral Beam Combining

Wavelength combining systems are an incoherent beam combining technique, usually favorable with respect to coherent combining due to the invariant beam patterns with the number of elements, the easier element-control requirements, and the more graceful degradation and easier scaling in fixed optical systems [14].
It combines beam having different wavelength by means of dispersive optical elements as shown in Figure 2.4, avoiding beam quality degradation at the expense of resulting beam spectral width.

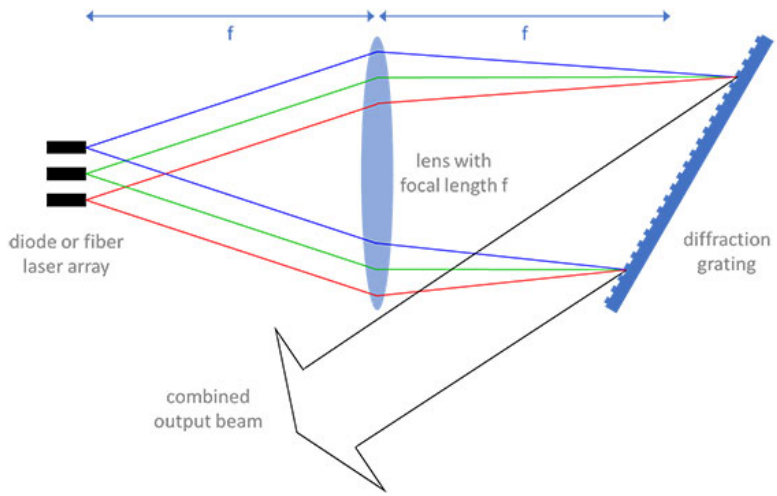

Figure 2.4: Setup for wavelength beam combination with a diffraction grating. Each wavelength has its own diffraction angle at the grating, and the emitters automatically tune to the wavelengths corresponding to their location.

Wavelength combining scales as

$$B \propto f_{\mathrm{g}} N \tag{2.4}$$

where f_{g} is an efficiency factor less than or equal to 1, which is similar to coherent beam combining. As already introduced, spectral combination allows a more graceful degradation with respect to coherent combination, where intensity scales as F^2 in fixed systems (if no reconfiguration is adopted). For example, considering a two element system, 50% drop is expected for wavelength combination system, 75% for coherent beam combining without adjustment, 50% for coherent beam combining with physical reconfiguration of the optics [14].
Moreover, wavelength combining systems are easily scalable (despite the difficulty of dichroic mirror realization), while coherent beam combined systems, optical-system changes are required to achieve the maximum on-axis intensity. As regards amplitude fluctuations, coherently combined systems are more largely affected in terms of efficiency and total power. If there are amplitude variations in wavelength-combined systems, there is no impact on the near- or far-field patterns and the on-axis intensity simply tracks the total power of the elements. A detailed analysis of the effect of amplitude variations has been done by Leger [15].

In conclusion, spectral beam combining seems to be the most efficient way for realizing a high power, high brightness diode laser for direct industrial applications at the current state of the art.

Chapter 3

Stabilization

The noise spectrum of the laser's frequency fluctuations leads to an effective linewidth of the laser, which conceptually describes the broadening of the laser spectrum around its central frequency.
The laser linewidth is dependent on the timescale over which it is evaluated, as a laser noise spectrum typically contains very different fast and slow components. Fast fluctuations, in a time less than the effective spectroscopic interaction time (typically tens or hundreds of microseconds), give rise to what is called the fast linewidth (or sometimes just linewidth); the low-frequency fluctuations (usually of larger magnitude) then cause jitter of this narrow spectral line in frequency space. Even slower changes often occur because of thermal effects, which can cause the laser's central frequency to drift.

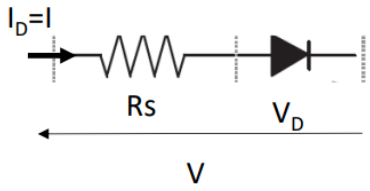

Figure 3.1: Simplified equivalent circuit model of a laser diode.

To better understand the nature of such fluctuations, It is necessary to introduce Wall Plug Efficiency as:

$$\mathrm{WPE} = \frac{\text{optical power out}}{\text{electrical power in}} = \frac{P_\mathrm{o}}{I^2 R_\mathrm{s} + I V_\mathrm{d,th}} \tag{3.1}$$

Given that, the dissipated power can be defined as $P_\mathrm{d} = P_\mathrm{in} - P_\mathrm{o}$. It is this dissipation that turns into heat with a consequent increase of temperature $\Delta T = Z_\mathrm{T} P_\mathrm{d}$. When not controlled, this power dissipation causes an increase in the junction temperature, leading to a non linear Power vs Current characteristics due to non radiative recombinations (Auger and Shockley-Read-Hall recombination) which cause higher internal losses and lower internal quantum efficiency η_i. The decrease of gain at fixed wavelength affect the

carrier density threshold.
On the other hand, the variation of refractive index with temperature affects the effective refractive index, giving rise to Red Shift (longer emission wavelength).

Moreover, random carrier and photon recombination and generation events produce spontaneous time variations in the carrier and photon densities which causes variation in magnitude of output power providing a noise floor.
Spontaneous emission and the above mentioned carrier density fluctuations turns into a variation of the lasing frequency. This laser linewidth at full width half maximum can be defined as:

$$\Delta\nu_{\mathrm{FW}} = (\Delta\nu)_{\mathrm{ST}}(1+\alpha^2) = \frac{\Gamma R_{\mathrm{sp}}^{'}}{4\pi N_{\mathrm{P}}}(1+\alpha^2) \tag{3.2}$$

where Γ is the gain coefficient, $R_{\mathrm{sp}}^{'}$ is spontaneous emission, N_{P} is photon density and α is the linewidth enhancement factor which is governed by the fluctuation of refractive index and gain in the active layer under carrier injection.

3.1 Stabilization scheme

In order to avoid noise and temperature fluctuations, the emission wavelength must be tuned at a specific frequency to avoid overlapping of spectrum in SBC constructing a feedback loop. Possible scheme are active or passive stabilizations.

These techniques can be used individually or in combination to achieve higher levels of stability and precision. The choice of technique depends on the specific application and the level of stability required.

There are several active techniques that are commonly used in various applications.

- As theoretically analysed in [16] and in [17], temperature stabilization can be achieved using a Peltier cooler or a thermoelectric cooler. However, there are some disadvantages of such approach like for example, power consumption. In fact, Peltier coolers can consume up to several watts of power. Moreover, they might experience thermal lag which can lead to slower response times and reduced stability. Nonetheless, the addition of a thermocooler could require additional space with respect to other techniques and no reduction of linewidth is expected with such approach.

- Current stabilization, on the other hand, does not require additional components mounted on the heatsink or module, however, they suffer from temperature variations and noise fluctuations requiring additional filtering or shielding to prevent interference. Since it consists of regulation of the injection current using a feedback loop based on the output power, it has a limited range of operation and could require periodic calibration due to component drift.

- In applications such as laser metrology or laser spectroscopy, Locking the laser diode frequency to a reference frequency through optical frequency locking, Pound-Drever-Hall locking can be advantageous. However, those technique can be expensive and complex to implement, particularly for high precision applications. They can be sensitive to changes in the environment such as temperature and vibrations, making it particularly inadequate for additive manufacturing.

- External cavity stabilization involves using an external cavity to stabilize the output of the laser diode. The external cavity can be a Fabry-Perot cavity, a diffraction grating, or a fiber Bragg grating. The output of the laser diode is coupled into the external cavity, and the feedback loop adjusts the cavity length to stabilize the output. It can provide high precision and high stability, but can be complex and expensive to implement.

- Passive external cavity stabilization is simpler and less expensive, but may be less precise and have limited correction capabilities. In passive external cavity stabilization, the laser diode is mounted within an external cavity that uses a passive stabilization mechanism, such as a diffraction grating or an etalon. The passive stabilization mechanism provides a stable reference for the laser diode, ensuring that the laser output remains stable and predictable. It is relatively simple and inexpensive to implement, with a lower degree of complexity compared to active external cavity stabilization. However, passive external cavity stabilization may be less precise than active stabilization techniques, with limited ability to correct for changes in the laser diode's temperature, current or other environmental factors. Even though it is less precise than active stabilization, it is particularly suitable for additive manufacturing and consumer goods.

3.2 External cavity

The spectral behaviour of laser diode strongly depends on the optical cavity. The electric field inside the cavity can be written as:

$$\mathrm{E}(x,y,z) = \hat{e}\sum_{\mathrm{m}}^{M} E_{\mathrm{m}}(x,y)e^{j\beta_{\mathrm{m}}z} \tag{3.3}$$

where $\hat{e}$ represents the polarization, M the total number of propagating modes, $E_{\mathrm{m}}(x,y)$ the m-th mode propagating along the z direction with a modal propagation constant β_{m} that takes into account the modal gain and the modal loss:

$$\beta = \frac{2\pi n_{\mathrm{eff}}}{\lambda} + \frac{j}{2}(\Gamma g - \alpha_{\mathrm{i}}) \tag{3.4}$$

Threshold is achieved when gain compensates propagation and mirror losses and the field replicates itself after a round trip:

$$R_1 R_2 e^{(\Gamma g_{\mathrm{th}} - \alpha_{\mathrm{i}})L} = 1 \tag{3.5}$$

The Barkhausen criterion can be further separated into a phase condition and an amplitude condition. The phase condition imposes the longitudinal modes that can be expressed as:

$$\lambda_{\mathrm{m}} = \frac{2n_{\mathrm{eff}}L}{m} \tag{3.6}$$

while from the amplitude condition the gain threshold is obtained:

$$\Gamma g_{\mathrm{th}} = \frac{1}{L} log\left(\frac{1}{R_1 R_2}\right) + \alpha_{\mathrm{i}} \tag{3.7}$$

There are only few modes that satisfy the laser threshold condition. When the gain reaches threshold, it doesn't increase anymore with current (Gain clamped at threshold) and the wavelength that satisfies the cavity round trip condition (both in phase and module) is the lasing wavelength or lasing mode.
Laser Diodes designed for high power are in general multi mode and have a much wider spectrum than single mode laser diode, which leads to small longitudinal intermode spacing around the lasing wavelength, poor wavelength selectivity of the mirrors, and non linear thermo-optical effects. As already mentioned, gain and therefore wavelength are a function of temperature and carrier density leading to red shifts with temperature increase.

To avoid such fluctuations an external cavity can be added with an additional wavelength selective mirror.

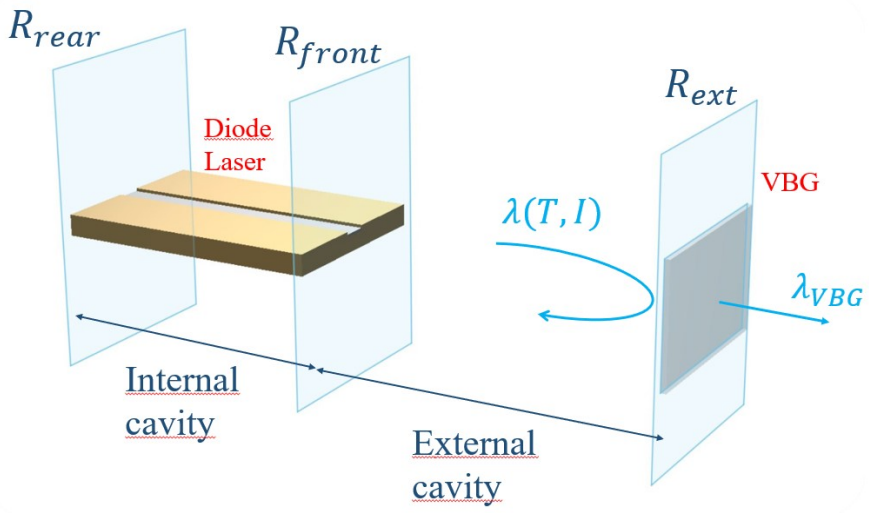

Figure 3.2: Structure of laser diode cavity and external cavity.

An equivalent reflection coefficient can be defined to represent the behaviour of the modified cavity taking into account the characteristics of the front reflector, the external reflector and the free space in between. This equivalent reflection coefficient can be computed from the transmission matrix resulting from cascading the transmission matrix

of the reflectors and the free space, or exploiting the scattering (S) matrix of the single elements. With reference to Figure 3.2, the equivalent reflection coefficient $r_{\text{eff}}(\lambda)$ can be expressed as:

$$r_{\text{eff}}(\lambda) = r_2 + \frac{t_2^2 r_{\text{ext}}(\lambda) e^{-2j\beta_{\text{ext}} L_{\text{ext}}}}{1 + r_2 r_{\text{ext}}(\lambda) e^{-2j\beta_{\text{ext}} L_{\text{ext}}}} = |r_{\text{eff}}(\lambda)|\, e^{j\theta_{\text{eff}}(\lambda)} \tag{3.8}$$

Given the reflectivity of both the front (R_{front}) and external (R_{ext}) cavities, three conditions can be met: unstabilized, semi-stabilized or stabilized laser emission. When R_{front} is much higher than R_{ext}, the external cavity contribution is negligible; if they are the same order, competition among cavities takes place and two wavelength sharing the same net gain appear in the laser spectrum. Finally, when the external reflector has an higher reflectivity with respect to the front reflector, the laser is stabilized at the emission wavelength imposed by the external cavity.

3.3 Impact of External Optical Feedback

External Optical Feedback (EOF) has many advantages if considered as a stabilization technique, if so it is defined intentional. However, it must be taken in account that it can become an important issue in high power diode laser applications and that can lead to accelerated or even sudden degradation.

In general, intentional or unintentional EOF can happen. Intentional feedback, e.g. from VBGs, is widely used for wavelength stabilization and wavelength tuning. On the other hand, unintentional feedback can start from micro-optical elements or fiber ends in fiber coupled modules, but also from non-absorbed pump radiation in diode-pumped laser systems or reflections from work piece surfaces in direct applications.

When laser radiation is reflected and hits the outcoupling facet, part of it can be absorbed leading to changes in the local charge carrier density and refractive index. The effect of such alteration is a modification of laser parameters and in particular, of the near field (NF) distribution. Those variations can cause a strong increase in the local power density at the outcoupling facet causing catastrophic optical mirror damages (COMDs). Up to date, there is no framework for the quantification of the maximum allowed EOF strength for reliable diode laser operation.

As already partially pointed out, EOF can impact different parameters such as laser threshold due to more photons in the active region consequently higher gain while the periodic modulation of refractive index causes different optical path lengths impacting both intensity and wavelength emission. Effects such as non-uniform intensity distribution with pronounced maxima and minima caused by non linear effects known as filamentation and beat-frequency of the internal and external cavity can be observed as spikes on the emission spectrum and intensity spectrum.

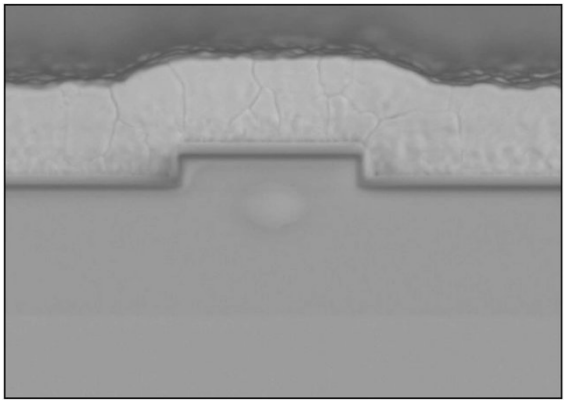

Figure 3.3: SEM view of the front facet of a laser diode which failed during vacuum operation by COMD [1].

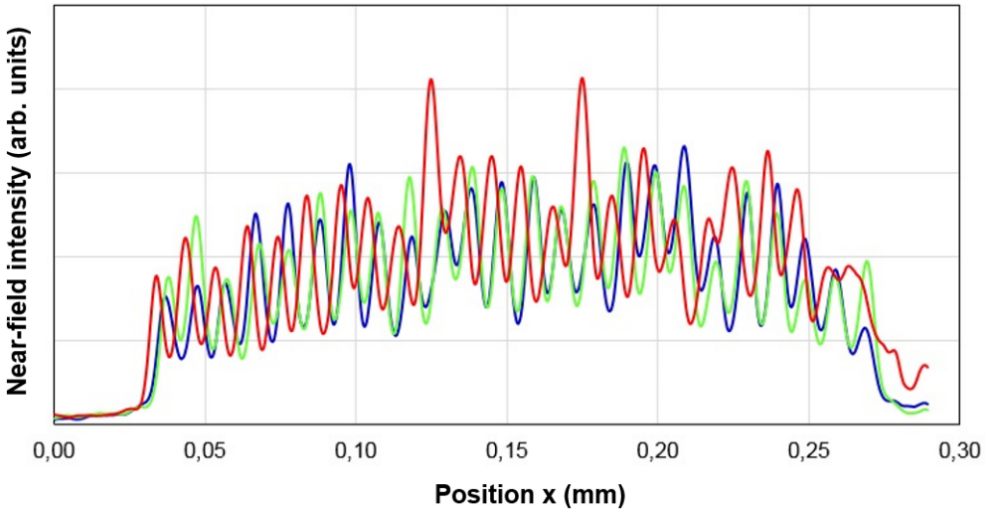

Figure 3.4: NF distribution of a BAL emitting at 880 nm with 4 mm cavity and 2.5% AR coating. The green line shows the NF distribution without EOF, the blue line with 10% general feedback, and the red line with wavelength selective feedback from a 10% VBG [2].

Device degradation starts at a specific location that is already pre-damaged or it has experienced extra load in terms of current or photon density even if it exceeded the COD threshold in one filament for few nanoseconds. This results in local heating or strain, reducing in general the lifetime of the device by doubling the degradation rate. However device degradation occurs in life tests after several hundred or thousand hours of operation in combination with another degradation mode: facet and/or mirror aging. In this case, the COD limit decreases with test duration and leads to a rapid increase of the degradation rate, when it reaches the test power. That means, facet stability is also a critical issue.

It is clear that the alteration of output parameters of a laser diode affected by intentional or unintentional EOF decreases with increasing reflectivity of the AR coating, because it reduces the quantity of radiation absorbed.

In general, the failure mode described, is even more critical for HPLD because they are more sensitive to wavelength-selective feedback compared to general EOF. CO(M)Ds can already occur during optical alignment or due to slight thermo-mechanical misalignment's in operation.

When dealing with unintentional or intentional external optical feedback, only a certain part of the back-reflected laser light is coupled into the waveguide layer due to the divergent emission of semiconductor laser diodes. The remaining part is absorbed either by defects in the substrate buffer and cap layers if the emission wavelength is longer than the substrate bandgap with no substantial heating of the device; or it is absorbed closely to the front facet if shorter wavelength are involved causing a strong heating of the outcoupling facet and heat distribution into the cavity.

In conclusion, further improvements of the facet passivation, the long-term facet stability, the facet temperature in operation and the maximum allowed power density of the AR coating are very helpful to reduce or avoid EOF induced degradation [2].

3.4 Fiber Bragg Grating

Fiber Bragg Gratings (FBG) are used to stabilize laser diode by refractive index variations inscribed into the delivery fiber core. The usually weak periodic refractive index variation can be expressed as:

$$n_{\mathrm{FBG}}^2(z) = n_0^2 + \delta n^2(z) \tag{3.9}$$

where $\delta n \ll n_0$ with n_0 being the refractive index of the unperturbed optical fiber core and δn the small periodic refractive index variation.

The wavelength stabilization via Fiber Bragg Grating can be analyzed by means of the Coupled Mode Theory. Without entering the details of theory, an analytical solution for single mode fibers can be found demonstrating that the phase matching condition in Equation 3.10 can be achieved, locking the emission wavelength.

$$\lambda = \frac{2n_{\mathrm{eff}}\Delta}{l} \tag{3.10}$$

If a multimode delivery fiber has to be studied, there is no more a single mode propagating, thus the phase matching condition can be satisfied not only by the forward and backward component of the same mode but also by the forward and backward component of different modes which gives rise to multiple reflectivity peaks. Therefore, locking of the laser diode in unexpected spectral range can take place.

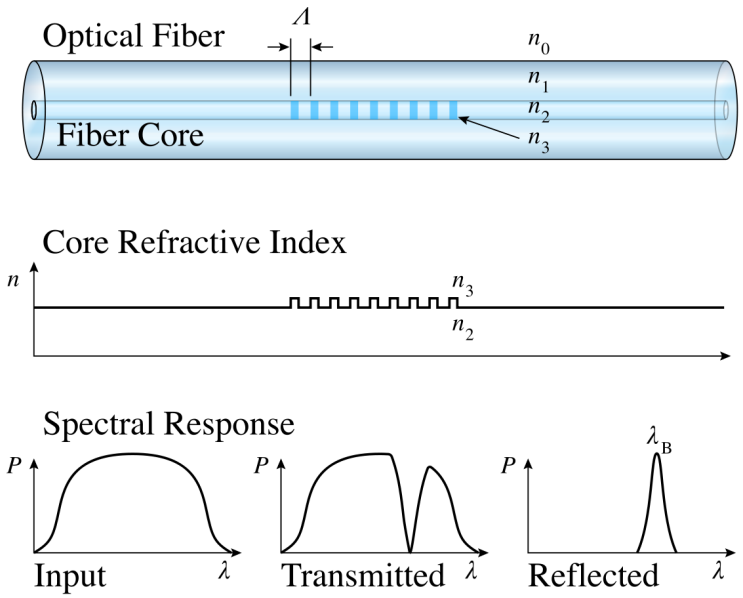

Figure 3.5: Fiber Bragg Grating structure, refractive index modulation and spectral response.

In general, phase mask based method or femtosecond laser pulses can be used to inscribe gratings into the fiber core. However, even if the former technique allows extremely precise refractive index modulations, it cannot be applied to very large core area fiber, while the latter one, allows a controlled spatial extension of the variation at the expense of poorer variation homogeneity.

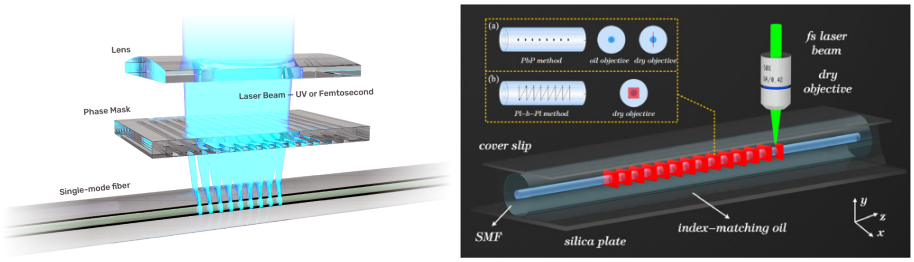

Figure 3.6: Phase mask method (left) and direct writing (right) schematic.

Even though FBG have the advantage of no scattering loss if ideally inscribed, they are difficult to realize for high power applications where optical losses due to the inscription method adopted must be reduced. Moreover, the adoption of fiber bragg gratings for high power blue laser diodes is still under investigations and is not a commercially available solutions for large scale productions.

3.5 Volume Bragg Grating

Volume Bragg gratings, also known as volume holographic gratings, refer to a type of Bragg grating that is inscribed inside a transparent material, such as a cube or parallelepiped. Unlike diffraction gratings, which are made on the surface of an optical element, or fiber Bragg gratings, which are written into the core of an optical fiber, volume Bragg gratings are three-dimensional structures that are distributed throughout the bulk of the material.

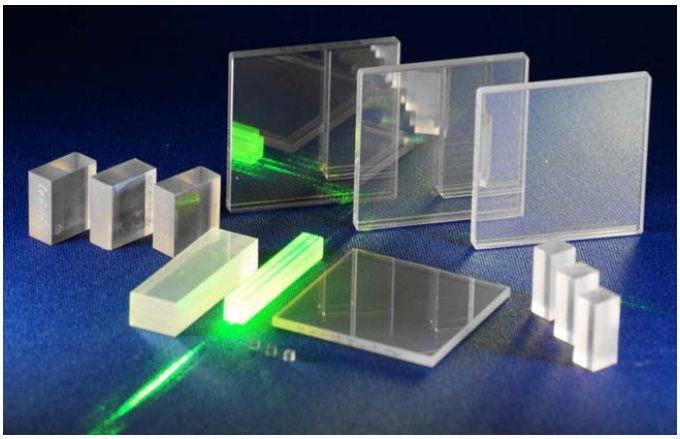

Figure 3.7: Commercial transmitting VBG.

Typically, volume Bragg gratings are fabricated by exposing photosensitive glass or crystal materials to an interference pattern generated by two or more coherent laser beams. The resulting grating structure consists of a periodic variation in refractive index, which diffracts light that is incident upon the grating at a specific angle, determined by the grating period and the refractive index modulation depth.

Volume Bragg gratings are typically designed with a very small grating period, usually below 1 µm, in order to obtain a narrowband spectral filtering effect, such as a bandwidth of 0.1 nm or lower. This can be achieved by reflecting light either directly back into the incoming beam or at a certain angle. In addition to reflection, there are also transmitting Bragg gratings (TBG), where the diffracted beams on the same side of the device are the transmitted beams.
The peak reflectance of a volume Bragg grating can vary significantly, from just a few percent to over 99%, depending on the length of the grating and the magnitude of the refractive index modulation. The shape and width of the reflection spectrum, also known as the filter shape, can be tailored to some extent.
The thickness of volume Bragg gratings is typically several millimeters, allowing for substantial beam radii of a few millimeters. This large beam area, in combination with the high optical damage threshold of multiple J/cm^2, allows for very high peak powers. Moreover, optical losses related to absorption or scattering of light are usually at a very low level, allowing these devices to be operated at high average power levels.

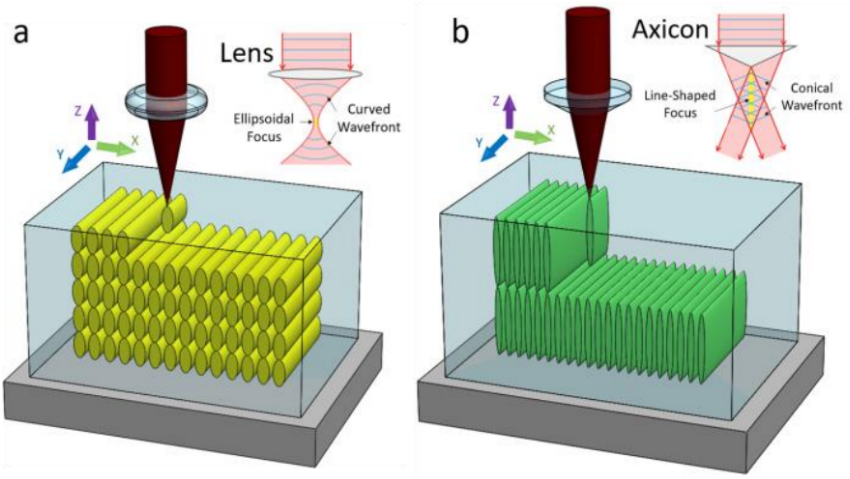

Figure 3.8: Schematic drawing of volume Bragg gratings fabrication approach by means of Gaussian laser beam approach(a) and Gaussian-Bessel laser beam approach(b) [3].

While most devices contain only a single grating, it is possible to have two or more Bragg gratings within the same volume of material. Chirped volume Bragg gratings (CVBG, CBG) are devices where the Bragg wavelength varies continuously along the device, rather than being constant. The purpose of the chirp can be to obtain a large reflection bandwidth or to achieve a certain amount of chromatic dispersion.

Volume Bragg gratings are widely used in optical devices and systems for their unique optical properties, such as narrowband spectral filtering and high diffraction efficiency. They are also known as bulk Bragg gratings, as the grating structure is distributed throughout the bulk of the material, and volume holographic gratings, as they are essentially holograms that are recorded in three dimensions.

When a volume Bragg grating is designed to operate at a particular wavelength and at the Bragg angle, it diffracts that wavelength most efficiently. However, when the incident angle of the light deviates from the Bragg angle, the diffraction efficiency decreases rapidly, leading to a reduction in the grating's performance.
The angular detuning can arise due to various factors such as the incidence angle of the light not being precisely aligned with the Bragg angle, the temperature of the grating being different from the design temperature, or mechanical stress on the grating due to external factors. In general, referring to Figure 3.9, it can be expressed as δ and impacts the diffracted wave vector k_{N} as:

$$k_{\mathrm{N}} = k_{\mathrm{M}} - mK + 2\delta \tag{3.11}$$

where $K = (0{,}0{,}2\pi/\Delta)$ is the grating vector when periodicity along the x-direction is assumed; m the order of diffraction, k_{M} the incident wave vector.

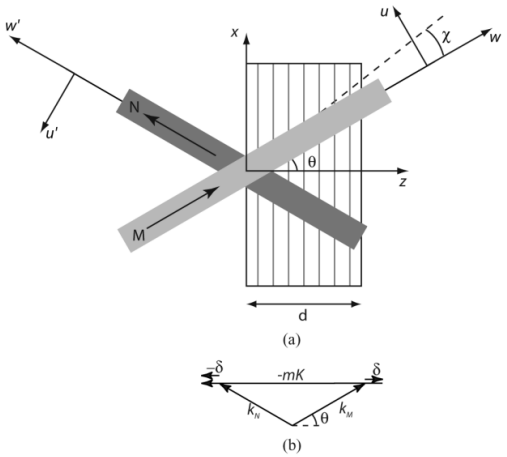

Figure 3.9: Illustration of the setup and definitions of coordinates in (a) real space and (b) momentum space.

Given that the diffracted and incident beam share the same wavelength:

$$k_{\mathrm{N}} = k_{\mathrm{M}} = \frac{2\pi n_0}{\lambda} \equiv \beta \tag{3.12}$$

and considered that momentum is preserved along the x-direction, the wave vectors can be rewritten as:

$$k_{\mathrm{N}} = \beta(\sin\theta\hat{x} - \cos\theta\hat{z}) \tag{3.13}$$

$$k_{\mathrm{M}} = \beta(\sin\theta\hat{x} + \cos\theta\hat{z}) \tag{3.14}$$

and the mismatch can be expressed as:

$$\delta = \frac{mK}{2} - \beta\cos\theta \tag{3.15}$$

Considering a perfect Bragg matching:

$$2k_{\mathrm{B}}\cos\theta_0 = mK \tag{3.16}$$

For a fixed wavenumber k_{B} the angular detuning $\delta\theta = \theta - \theta_0$ at normal incidence becomes:

$$\delta\theta = \sqrt{\frac{2\delta}{k_{\mathrm{B}}}} \tag{3.17}$$

while for oblique incidence ($\theta_0 > \delta\theta$) the angular detuning becomes:

$$\delta\theta = \frac{\delta}{k_{\mathrm{B}}\sin\theta_0} \tag{3.18}$$

As it has been demonstrated, angular detuning has different properties for normal or oblique incidence and it can significantly affect the performance of volume Bragg gratings,

leading to reduced efficiency and degraded spectral and spatial filtering properties as it will be later discussed. Therefore, it is essential to carefully control the alignment and temperature of the grating to ensure optimal performance.
Moreover, a wavenumber detuning $\delta k \equiv \beta - k_{\mathrm{B}}$ can be defined for fixed angle of incidence ($\theta = \theta_0$):

$$\delta k = -\frac{\delta}{\cos\theta_0} \tag{3.19}$$

Similar to angular detuning, wave number detuning can also significantly affect the performance of volume Bragg gratings. Additionally, volume Bragg gratings can be designed to have a broader spectral bandwidth, which can reduce the sensitivity of the grating to wave number detuning.

To better understand the working principle of volume bragg gratings, an equivalent transmission line model can be adopted if the incident beam wavelength is much smaller than the VBG thickness, conserving at any point of the stack the transverse component of the wave vector $k_{\mathrm{x}} = \xi$ and assuming the fields in the grating to only have a z-dependence. Given those assumption, the evolution of each incident wave inside the grating can be expressed as:

$$\begin{cases} -\dfrac{dV}{dz} = jk_{\mathrm{z}} Z_\infty I \\ \\ -\dfrac{dI}{dz} = jk_{\mathrm{z}} Y_\infty V \end{cases} \tag{3.20}$$

where $k_{\mathrm{z}} = \sqrt{(\dfrac{2\pi n}{\lambda})^2 - \xi^2}$ and $Y_\infty = \dfrac{1}{Z_\infty}$. Considering the decomposition in TE (or s-polarized) and TM (or p-polarized) waves, Equation 3.20 can be written in terms of traveling waves as:

$$V(z,\xi) = V_0^+(\xi)e^{-jk_{\mathrm{z}}z} + V_0^-(\xi)e^{jk_{\mathrm{z}}z} \tag{3.21}$$

$$I(z,\xi) = I_0^+(\xi)e^{-jk_{\mathrm{z}}z} + I_0^-(\xi)e^{jk_{\mathrm{z}}z} \tag{3.22}$$

and the Fresnel reflection coeeficient can be computed at each interface as

$$\rho_l = \frac{Z_{\mathrm{inf,i}} - Z_{\mathrm{inf,i-1}}}{Z_{\mathrm{inf,i}} + Z_{\mathrm{inf,i-1}}} \tag{3.23}$$

where $Z_{\mathrm{inf,i}}$ and $Z_{\mathrm{inf,i-1}}$ can be computed as $\dfrac{\omega\mu}{k_{\mathrm{z}}}$ or $\dfrac{k_{\mathrm{z}}}{\omega\epsilon}$ according to the polarization of the incident light. The reflection coefficient Γ_1 of the cascade of M dielectric layers surrounded by an infinite medium can be computed back-wards with an iterative algorithm as

$$\Gamma_l = \frac{\rho_1 + \Gamma_{1+1}e^{-2jk_{\mathrm{z,1}}L_1}}{1 + \rho_1\Gamma_{1+1}e^{-2jk_{\mathrm{z,1}}L_1}} \qquad l = M, M-1, ...1 \tag{3.24}$$

and the reflectivity of the stack is:

$$R(\lambda) = |\Gamma_1(\lambda)|^2 \tag{3.25}$$

In the case of a VBG, the optical notch filter is made by a periodic variation of the refractive index obtained from a binary stack of M dielectric layers with 0.25 optical thickness. To obtain a narrow-band behaviour, a small refractive index variation of the order of few percents is preferred. With such small difference between the high and low refractive index layer, it is possible to demonstrate that an high number of bilayers are needed to achieve high reflectivity.
Assuming that the surrounding medium is air, it can be shown that, at the peak wavelength and for normal incidence, the reflection coefficient Γ_1 of the stack is

$$\Gamma_1 = \begin{cases} \dfrac{(\frac{n_\mathrm{H}}{n_\mathrm{L}})^{2M} - 1}{(\frac{n_\mathrm{H}}{n_\mathrm{L}})^{2M} + 1} & \text{if M even} \\ \dfrac{1 - (\frac{n_\mathrm{H}}{n_\mathrm{L}})^{2M} n_\mathrm{H}^2}{1 + (\frac{n_\mathrm{H}}{n_\mathrm{L}})^{2M} n_\mathrm{H}^2} & \text{if M odd, } n_1 = n_\mathrm{M} = n_\mathrm{H} \end{cases} \tag{3.26}$$

with λ_{peak} being the central wavelength of the reflected band, $n_\mathrm{H} > n_\mathrm{L}$ the high and low refractive index, respectively. Once the reflectivity is computed, it can be inserted into Equation 3.8 replacing R_2 in Equation 3.7 to determine the behavior of a given laser diode when such a Bragg grating is used as the external reflector.

3.6 Experimental Results

The aim of the test performed in laboratory is to prove the practicability of locking via Volume Bragg Gratings and check the robustness with respect to current and temperature shift. The set up build in laboratory is composed of:

- the 30W blue multi-emitter module by Convergent mounted on a cold plate by means of thermal foil and secured by screws;
- The 444 nm center wavelength VBG, with a 40% reflectivity;

In order to properly align the VBG, SmarAct high precision robotic positioning system with 6 Degree Of Freedom has been employed to obtain a positioning accuracy of microns.
The working set up is shown in Figure 3.10.

The spectra and optical power measurement are captured using Avantes spectrometer and Thorlabs power meter.

To initiate the stabilization process, the first step involves characterizing the module that requires stabilization. This is accomplished by extrapolating the PI curve and wavelength shift through measurements of power and emission wavelength, while changing the driving current. The resulting data is plotted in Figure 3.11 where a total shift of almost

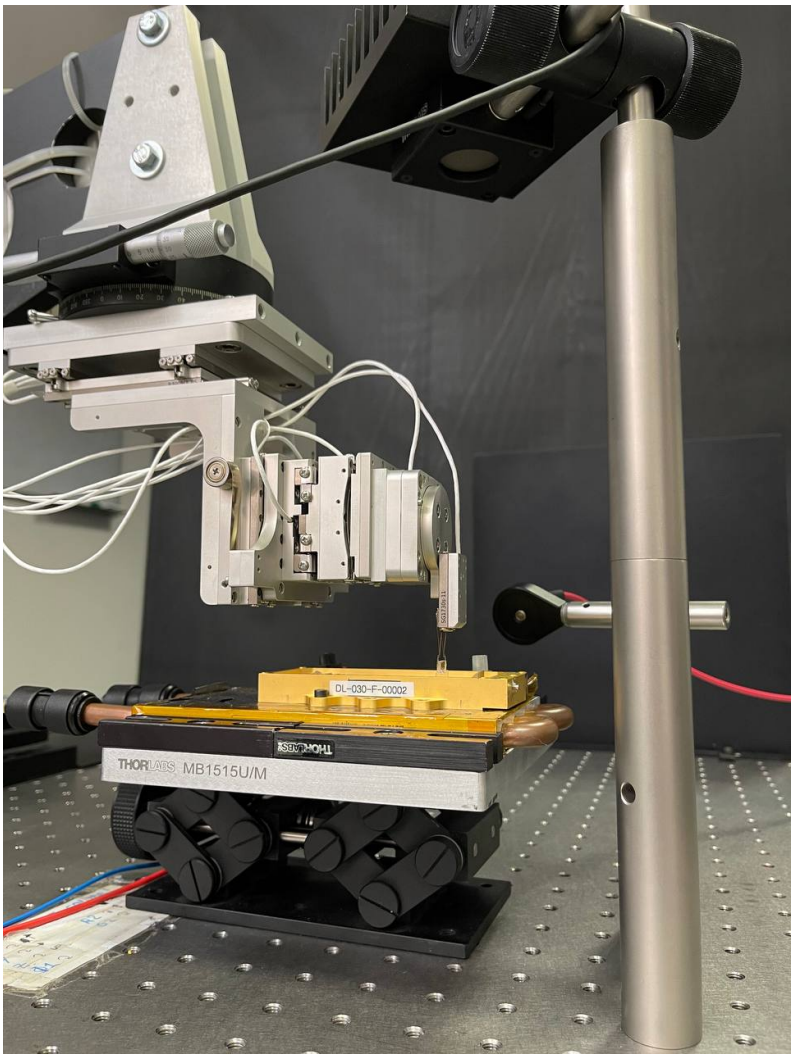

Figure 3.10: Working set up with the 30W blue multi-emitter, the Robotic Positioning System holding the VBG, Power meter and Spectrometer to capture data.

4 nm can be observed. Understand its behavior under different operating conditions helps in designing an effective stabilization system.

Once the suitable VBG has been chosen such that the narrow bandwidth matches the laser's wavelength and the temperature sensitivity has been checked to withstand the laser's output power, the diffraction grating can be placed inside the module by means of the High precision positioning system. The mounting should be stable and precise to prevent any movement and misalignment.

The initiation of the locking process can be readily observed by a significant increase

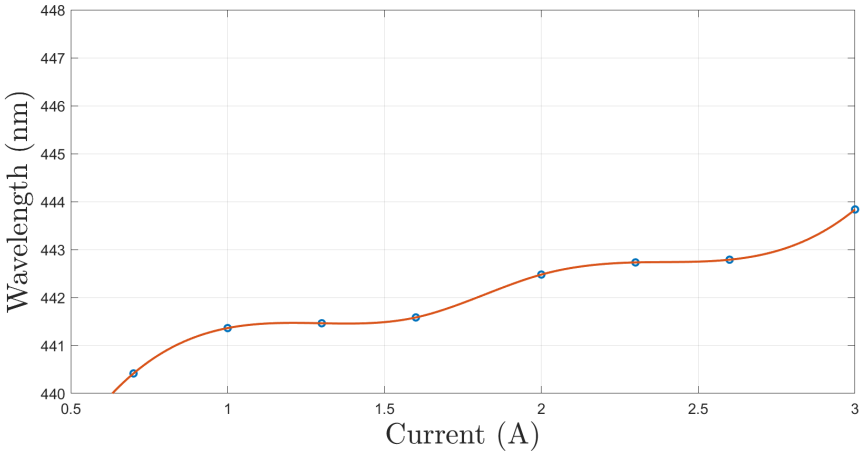

Figure 3.11: Wavelength shift due to driving current without stabilization at working temperature $T = 22\,^{\circ}\mathrm{C}$.

in the intensity of the light emitted from the chip on carrier and the emergence of a secondary peak in the spectrum, which starts to rise at the wavelength of the volume Bragg grating (VBG) peak. Under such circumstances, the reflectivity of the external cavity becomes comparable to or is of the same order of magnitude as that of the front facet. As a result, a competition between the lasing and the VBG wavelength begins. By making fine adjustments to reduce the losses resulting from misalignment, the reflectivity of the external cavity gradually override that of the internal cavity, leading to stabilization of the system.

The characterization of wavelength shift due to driving current is performed once again and it is reported in Figure 3.13. The maximum shift observed is lower than 0.5 nm.

For comparison purpose, the wavelength shift is reported for both the stabilized and non stabilized module in Figure 3.14.

Considering that the working temperature can drastically impact stabilization and wavelength shift, characterization of the module prior stabilization has been performed once more changing the cold plate temperature. Acting on the cold plate it is possible to simulate a cooler or warmer environment and conduct repeatable experiments. The re-characterization is essential to ensure that the stabilization system can compensate for any temperature fluctuations that may occur during the laser operation.

Wavelength shift due to temperature fluctuations are reported in Figure 3.15. The deterioration due to high temperature of multi-emitter modules can lead to a decrease in the device's performance, reliability, and lifespan. the main mode of degradation in laser diode is due to defects in the active inner region of the laser, which can result from growth of dislocations, facet degradation due to oxidation, electrode degradation due to metal diffusion, bond degradation and heat sink degradation. This defects, combined

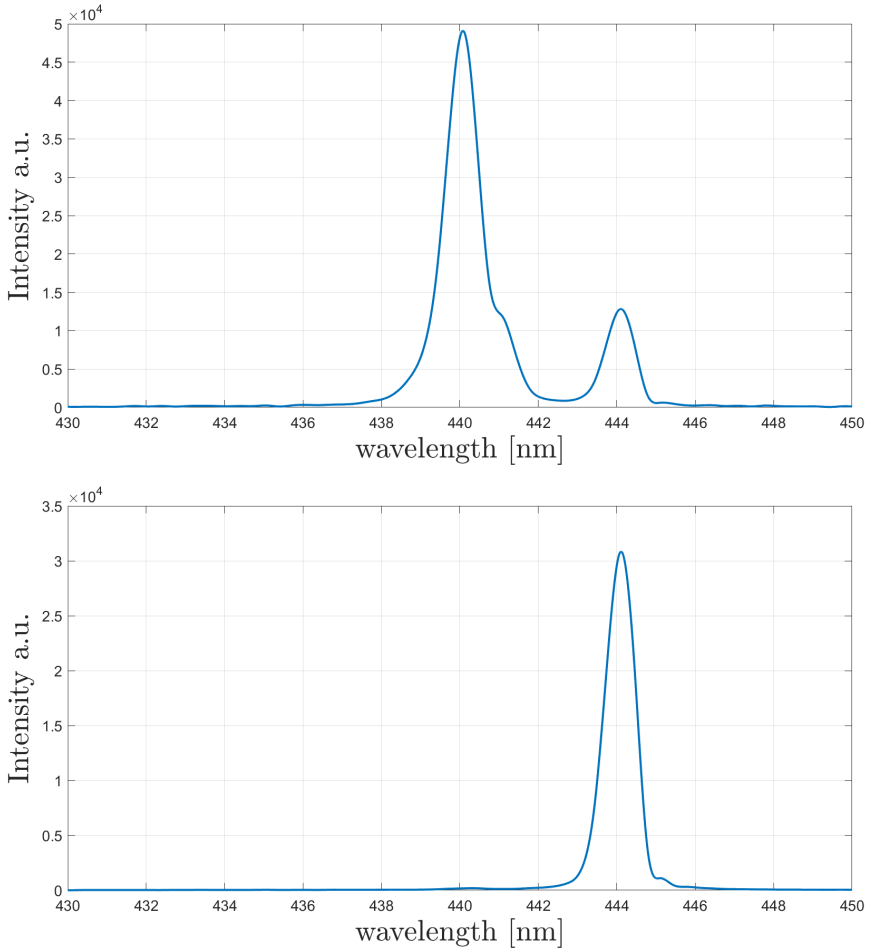

Figure 3.12: Spectrum of a semi-stabilized (top) and of a stabilized (bottom) multi-emitter module.

with increased current, temperature, light output, can further accelerate degradation. Therefore, it is crucial to keep the device operating at a suitable temperature to prevent or minimize such deterioration. Considering the safe operation temperature stated in the datasheet, the temperature variation is limited to 35 °C.

As can be observed from Figure 3.15, stabilization works properly in the temperature working regime.

The measurement of linewidth at Full Width Half Maximum (FWHM) has been reported in Figure 3.16. The reported behaviour is not accurate due to the limited resolution of the spectrometer employed. The minimum resolution of 0.335 nm has certainly affected the acquisition. It must be emphasized that its primary purpose is to provide a record of the measurement rather than to serve as a definitive representation of the actual linewidth. In summary, the reported results should be interpreted with caution

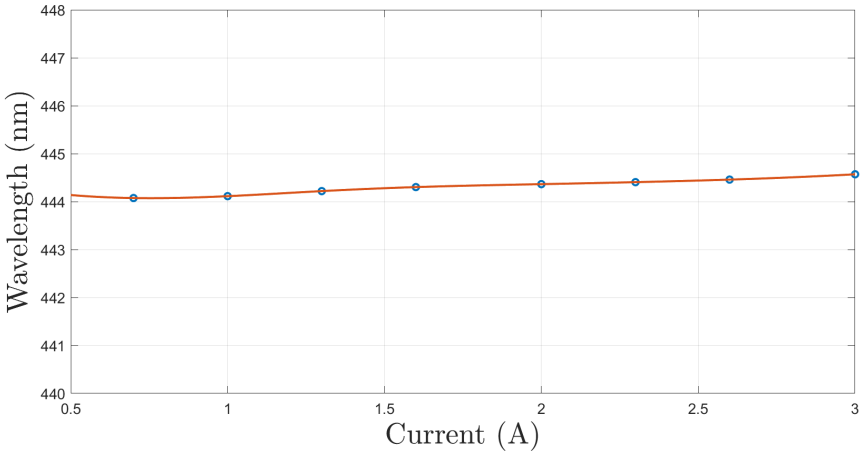

Figure 3.13: Wavelength shift due to driving current of the stabilized module at working temperature $T = 22\,^{\circ}\mathrm{C}$.

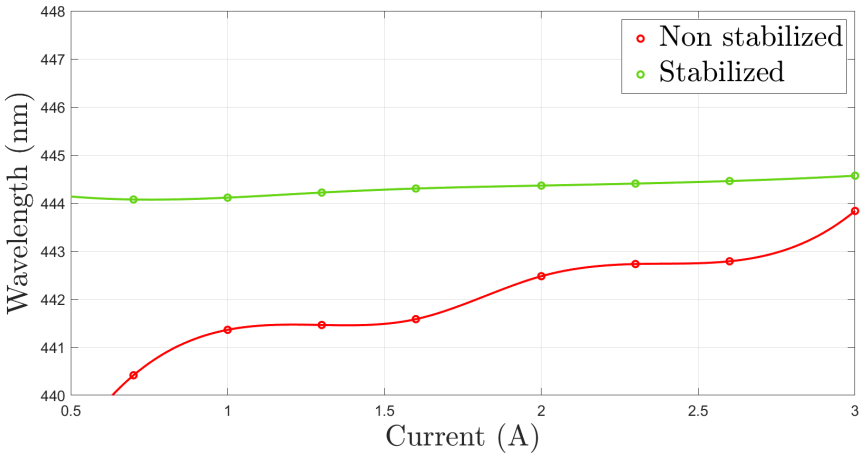

Figure 3.14: Wavelength shift due to driving current for stabilized (green) and non stabilized (red) module at working temperature $T = 22\,^{\circ}\mathrm{C}$.

due to the constraints imposed by the spectrometer's limited resolution.

Finally, PI curves of both stabilized and non stabilized modules are reported in Figure 3.17. A decrease in laser power output by 15% has been observed upon insertion of an external cavity. The reasons for this reduction can be attributed to several factors, including absorption, reflection, and scattering losses. However, lowering the diffraction efficiency of the grating it is possible to reduce losses and increase optical power at the cost of requiring more precise alignment of the external cavity.

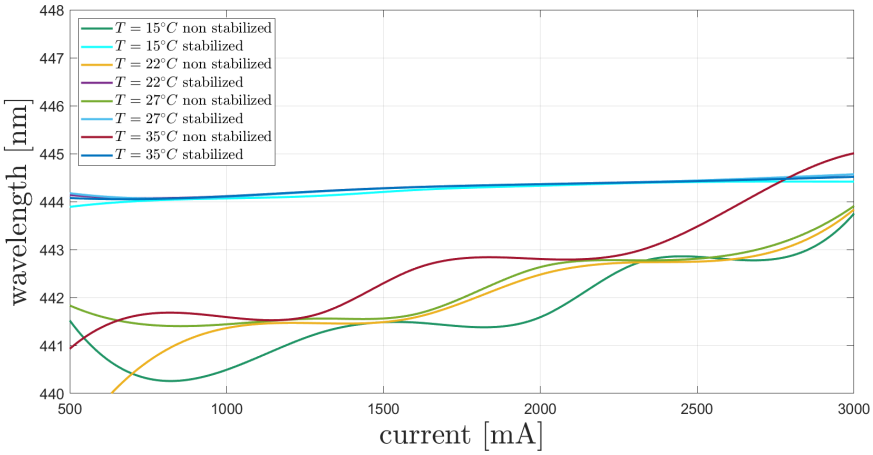

Figure 3.15: Wavelength shift due to driving current for stabilized and non stabilized module at different working temperature.

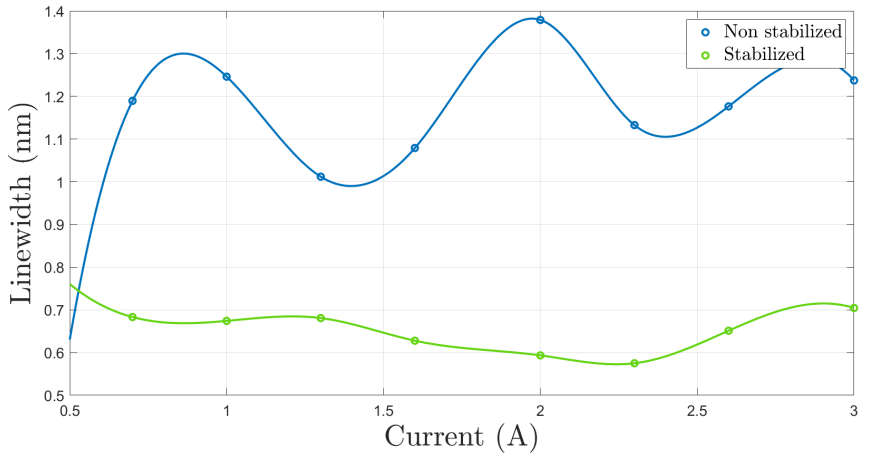

Figure 3.16: Variation of the linewidth of the laser as a function of the driving current applied to the non stabilized (blue) and stabilized (green) module.

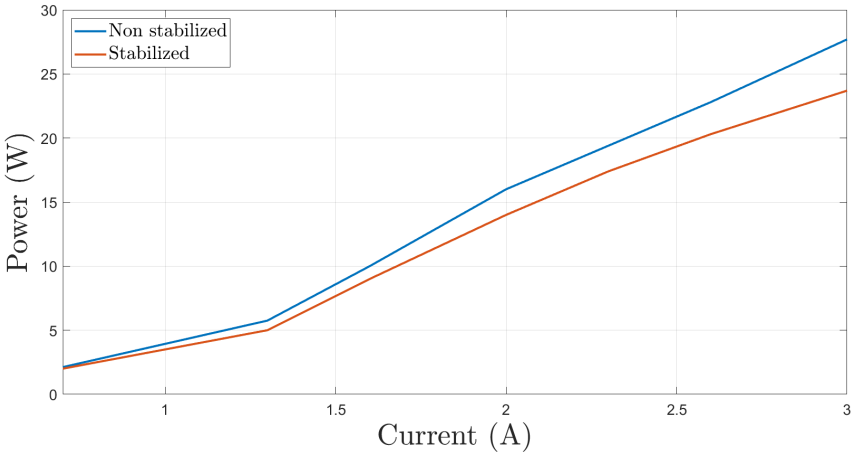

Figure 3.17: PI curves of stabilized and non stabilized module at $T = 22\,^{\circ}\mathrm{C}$.

3.6.1 Thermal analysis

For completeness, temperature monitoring of the Volume Bragg Grating has been performed. A thermal camera is firstly been used to capture the temperature increase of the diffractive element. However, due to limited working space between the VBG and the package, the temperature of the element could not be isolated from the packaging reflections. Therefore, a different set up has been built up to measure the heating of the VBG outside of the module package as reported in Figure 3.18. An additional acquisition was performed via Fiber Bragg Grating to double-check the registered temperature.

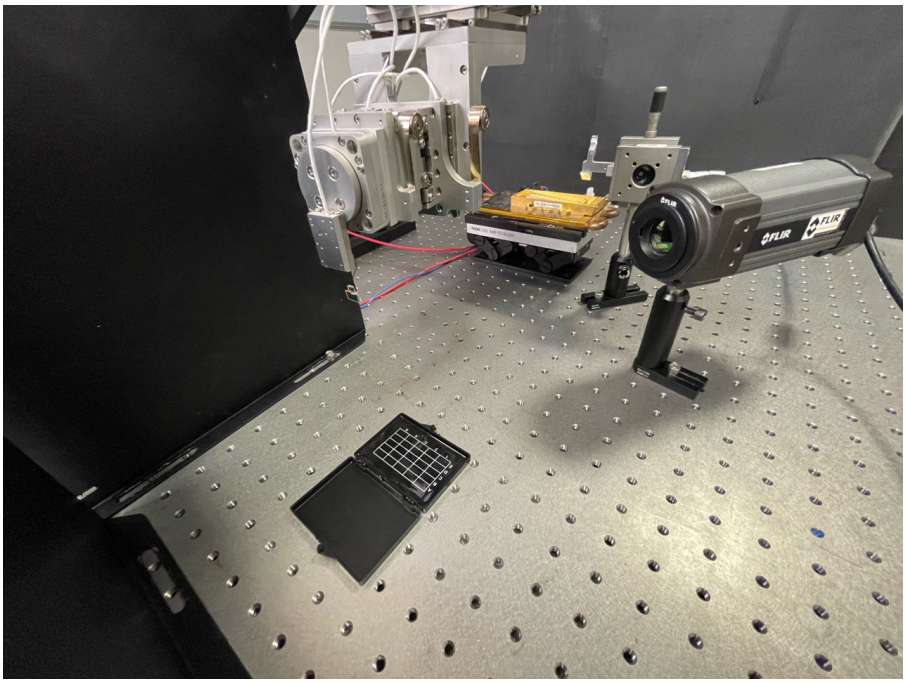

Figure 3.18: Set up for thermal measurement built in laboratory. The module mounted on a cold plate, with two return mirror, FLIR thermal camera and the VBG hold by means of the robotic positioning system.

As pictured in Figure 3.19 the ends of a fiber has been glued to the VBG in such a way that the grating inscribed in the fiber core is in contact with the glass. With such configuration, it is possible to record temperature increase observing the Bragg wavelength shift. The Bragg wavelength is determined by the period and refractive index modulation of the FBG. Changes in temperature can cause a shift based on the thermo-optic coefficient of the fiber, which characterizes the change in the refractive index of the fiber with temperature.

Given an FBG with $10\,\mathrm{pm}\,^{\circ}\mathrm{C}^{-1}$ it has been possible to collect the temperature trend reported in Figure 3.20. The initial measurement has been performed driving the module at 2 A, with 16 W optical power hitting the VBG's surface.

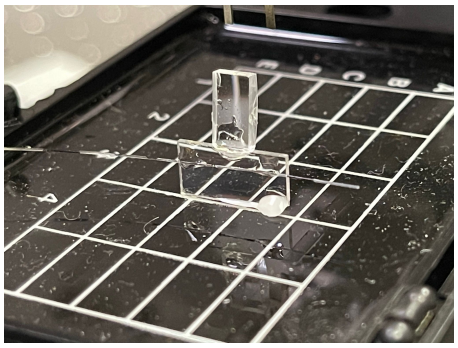

Figure 3.19: Fiber with FBG glued onto the VBG.

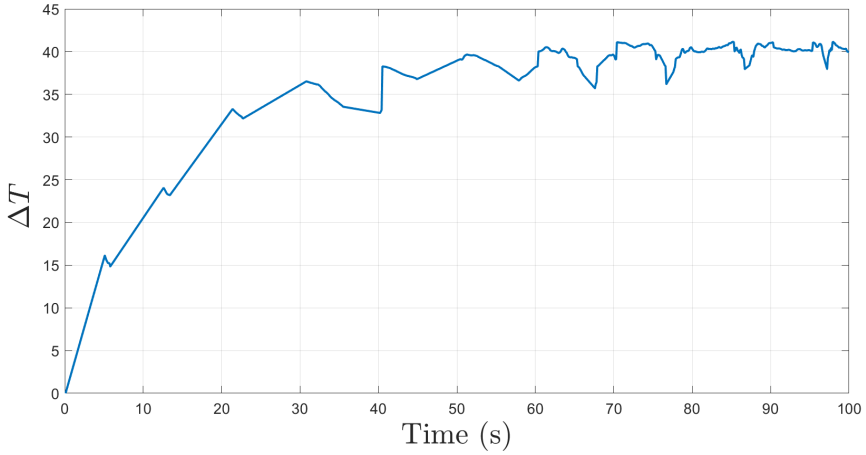

Figure 3.20: Temperature increase of the VBG hit by 16 W measured with an FBG.

The recorded temperature increase is in line with the measurement acquired with the thermo camera employed as depicted in Figure 3.21.

As a consequence, a simplified thermal model [18] has been tested in COMSOL Multiphysics. The geometry has been approximated to a 12 mmx6 mmx1 mm block having the same dimension of the VBG tested for stabilization. The grating is subjected to a Gaussian laser beam propagating perpendicular to the main plain of the grating and passing through the volume of glass. The geometry tested is reported in Figure 3.22.

In order to account for the heating of the Volume Bragg Grating (VBG) by the laser beam, a *Heat Source* model was introduced for the domains of the VBG. This model utilized a Gaussian beam distribution, which was modeled using the *Geometrical Optics physics*. In addition, a convective heat flux was defined on all boundaries, assuming natural air cooling of the VBG and an initial temperature of 20 °C.

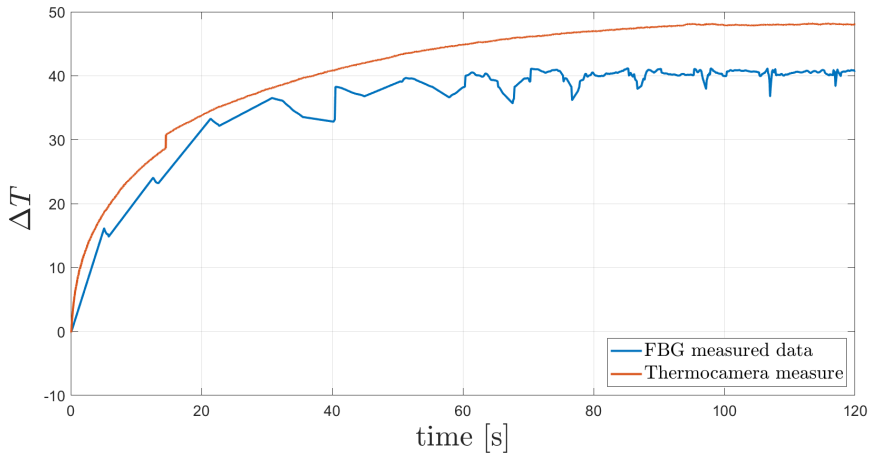

Figure 3.21: Temperature increase of the diffractive element monitored by means of a FBG (blue curve) and thermocamera (red curve).

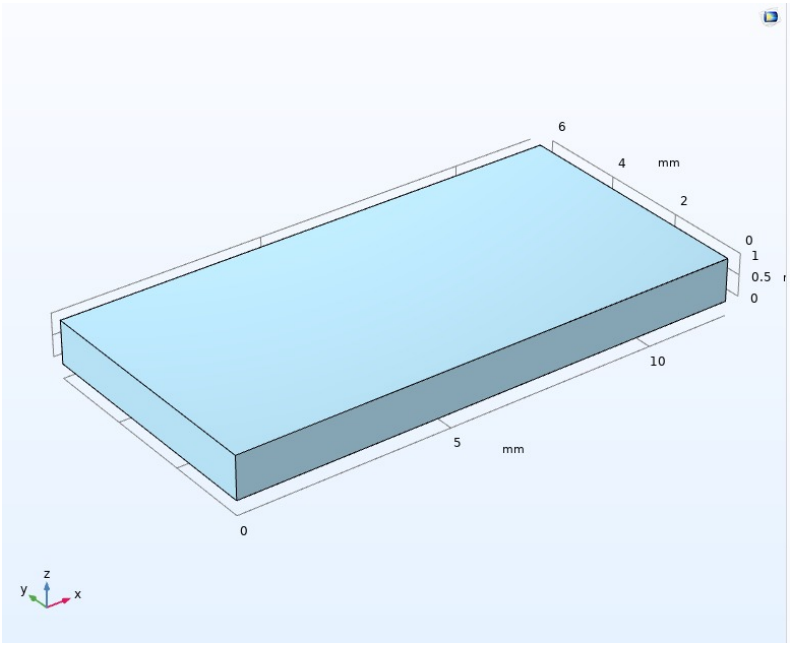

Figure 3.22: Geometry implemented in COMSOL Multiphysics.

It is worth noting that PTR glass is a relatively new material that is not widely known outside of specialized research groups and companies working with it. Therefore, in order to create a comprehensive model with corresponding material characteristics, a specific material was created for the purpose of using parameters that are specific to PTR glass. These parameters are reported in Table 3.1.

Table 3.1: Material characteristics of Photo-ThermoRefractive glass.

	value	unit of measure
Coefficient of thermal expansion	$9.5 \cdot 10^{-6}$	1/K
Heat capacity at constant pressure	840	$J/(kg \cdot K)$
Density	2500	g/m^3
Thermal conductivity	1.05	$W/(m \cdot K)$
Real refractive index	1.4891	dimensionless
Imaginary refractive index	$f(\alpha)$	dimensionless

The imaginary refractive index defined in Table 3.1 is related to the imaginary absorption coefficient by:

$$n_{\mathrm{i}} = \frac{\lambda \alpha}{4\pi} \tag{3.27}$$

where n_{i} is the imaginary refractive index, while α is the absorption coefficient. Due to the non specified absorption coefficient of PTR glass at 444 nm, the simulation has been adapted to be consistent with the acquired measurements.

The obtained heating is reported in Figure 3.23 where surface heat distribution has been plotted after 100 s of laser light exposure. The relative heating curve is reported in Figure 3.24 and for comparison purpose, it has been plotted on the same graph with the measurement in Figure 3.25.

It is particularly important to monitor VBG heating to prevent unwanted wavelength shift due to changing in the refractive index of the material. If the registered gradient cannot be acceptable for the stabilization requirement or the datasheet specifics, a proper cooling system should be designed.

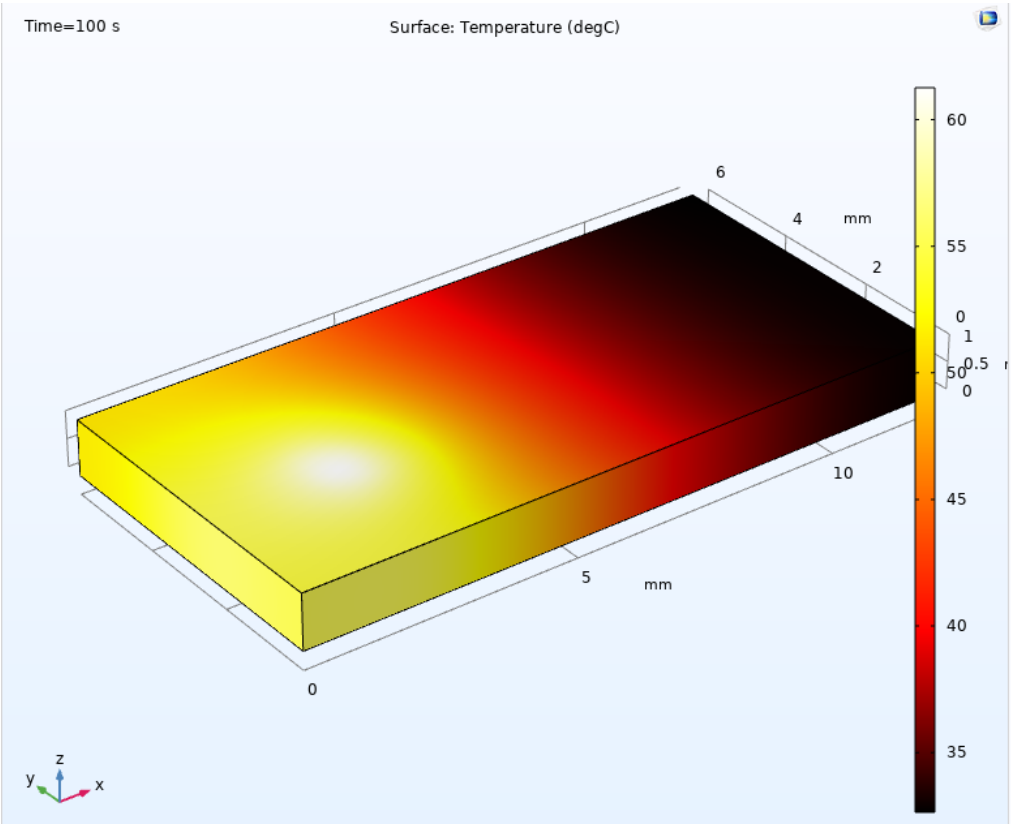

Figure 3.23: Surface heating of the VBG after 100 s exposure to 16 W laser blue light.

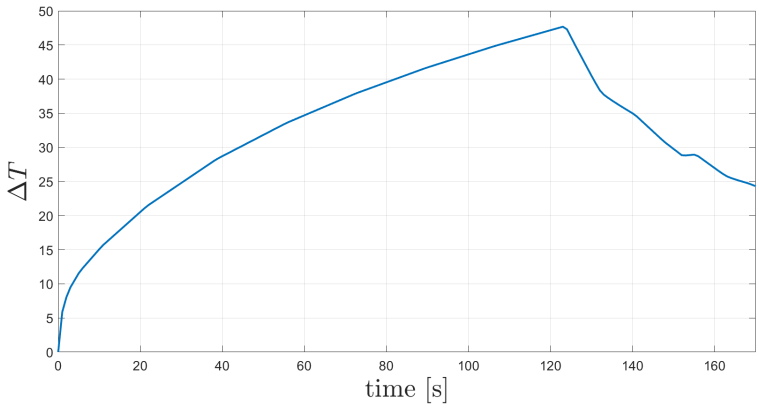

Figure 3.24: Simulated temperature increment of the VBG after 125 s exposure to 16 W laser blue light. Only the peak temperature is reported.

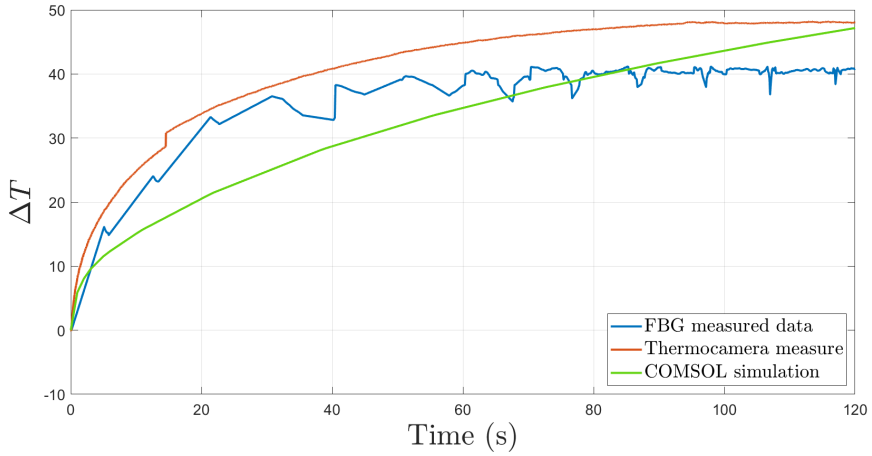

Figure 3.25: Temperature increment of the VBG due to 16 W laser blue light. Comparison between the simulated and recorded data.

Chapter 4

Spectral beam combining: Overview

Incoherent Wavelength Beam Combining (WBC), also known as spectral beam combining, is made of array of elements that operate at different wavelengths, and one or more dispersive optical elements used to overlap the different beams. The power of the emitter increases as the number of combined elements, just like spatial beam combining, but on the other hand, the beam quality of the final output beam equals the beam quality of the single emitter. Consequently, the brightness increases as the number of combined elements increases. The fundamental requirement for such behaviour is that the spectra of the combined elements not overlap with each other. If an overlap takes place, the beams will interfere and, to properly combine them, a precise control of the phase would be required.

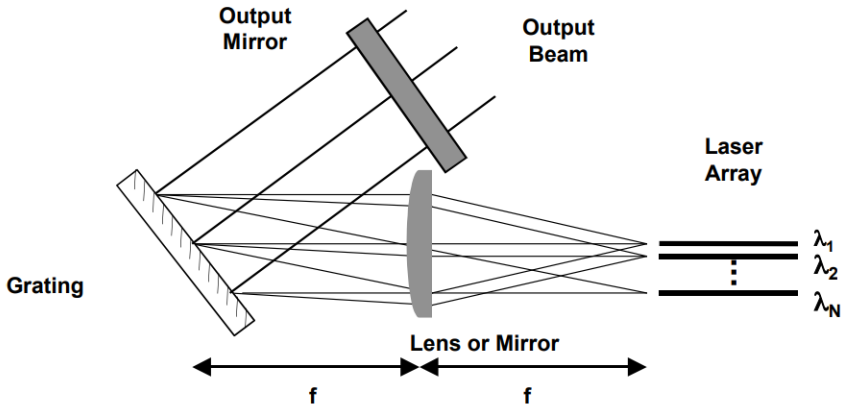

Figure 4.1: Wavelength-combining implementation invented at MIT Lincoln Laboratory using an external cavity containing a grating.

4.1 Gratings

The number of elements that can be combined is limited by the grating resolution. The dispersive element sets the spectral separation between the emitters while the laser's non zero spectral variance, imposes a transmission flat band $\Delta\lambda_T$ and a reflection flat band $\Delta\lambda_R$ respectively wider than the transmitted and reflected beam spectra. Moreover, HPLDs are strongly dependent on temperature. Red shift and spectral full width at half maximum increase can be observed with increasing temperatures, which should be taken into account when designing the combining element. A way to avoid such fluctuations is to stabilize the emission using VBGs or other stabilization technique's discussed in chapter 3. Another limitation is the need to keep the optical intensity under a critical value to avoid optical damage and thermo-optic distortion while maintaining high beam quality.

WBC architectures can be classified based on the frequency spacing(coarse or dense) or on the combining element(serial or parallel). In the serial approach, N-1 combiners are used to combine N beams with aligning complexity that grows as the number of elements increases. On the other hand, parallel approach requires only a single combining element.

4.1.1 Reflective Volume Bragg Gratings

Reflective Volume Bragg Gratings (RBG or Reflective VBG) represents a possible solution for dense combining scheme. The principle behind them is based on diffraction through the crystal's lattice. When the Bragg condition is met, light striking the surface of a VBG is reflected. Typical spectrum of a reflective VBG is shown in Figure 4.2. They can have diffraction efficiencies close to 100%, and if recorded in a suitable material that can have very low losses, they are particularly suitable for high power laser applications. Due to the absence of angular dispersion and the fact that they can be made to be very wavelength selective, they are a good optical element for implementation in the SBC system.

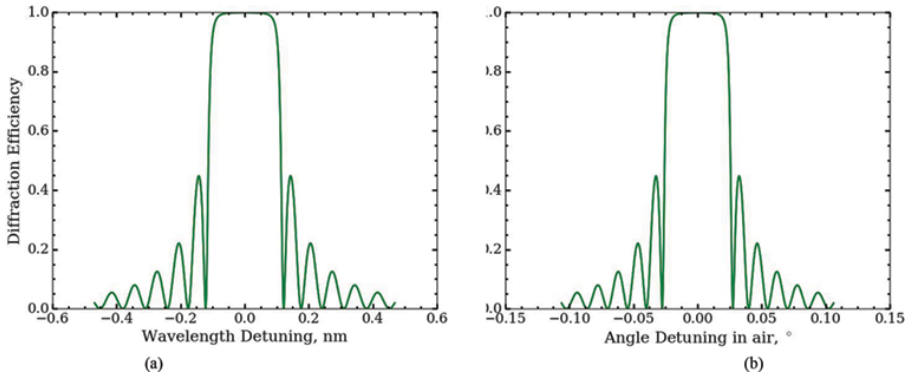

Figure 4.2: Wavelength (a) and angular (b) response for an RBG. The proposed spectrum refers to a VBG 5.5 mm thick, 20° tilted, which has a 240 ppm refractive index modulation.

The VBG in Figure 4.3 reflects wavelength λ_1 when it satisfies the Bragg condition at a given angle but transmits wavelength λ_2 with minimal losses if it matches with one the VBG minima. In this way, the diffracted beam λ_1 and the transmitted beam λ_2 can emerge overlapped and collinear. When using reflective VBGs for spectral beam combining, it is imperative to ensure as high as possible diffraction efficiency for the diffracted beam and minimal diffraction efficiency for the transmitted beam.

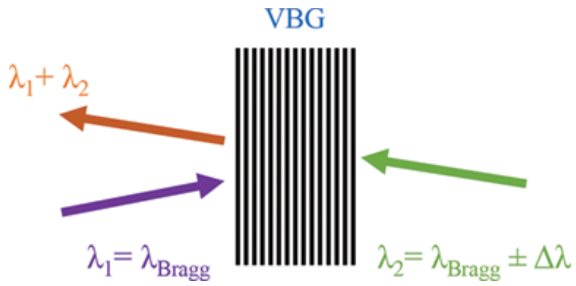

Figure 4.3: Schematic description of two-beam spectral combining setup using RBG as a combining element.

This approach for SBC can be extended where several VBGs are used to combine more than two laser beams. Such system was presented at the SPIE Photonics West conference in 2011 [19], where a five-channel SBC system using reflective VBGs has been demonstrated. The system had channel separation of 0.25 nm between adjacent wavelengths with a total combined power of 0.75 kW within a 1 nm spectral range. Figure 4.4 shows the design of the setup. To effectively combine high power beams with such a narrow spectral separation, very precise control of the VBG resonant wavelength had to be implemented. The most common method of tuning the resonant wavelength is by angular tuning of the VBG. However, due to the narrow angular selectivity of the VBG, mechanical tuning becomes a challenge and is impractical at high output powers.

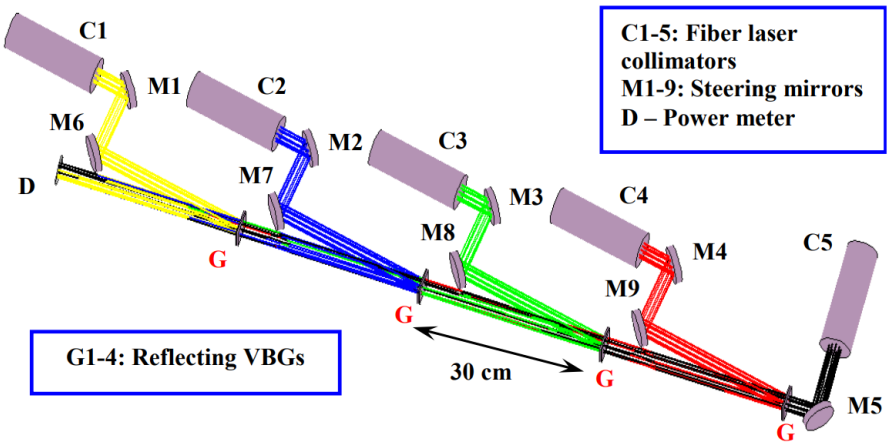

Figure 4.4: 5-channel spectral beam combining scheme implemented by using reflecting VBGs.

An alternative approach proposed by Ivan Divliansky et al. is thermal tuning [20]. By changing the temperature of the VBG, the glass expands or contracts, leading to changes of the period of the VBG and hence the resonant Bragg wavelength. This thermal method of tuning the resonant wavelength has much greater resolution than angle tuning and, once implemented, could be controlled electronically via thermoelectric coolers (TECs). With this tuning method, it is possible to maintain peak combining efficiency of the system regardless of the power operation range, without mechanical realignment.

4.1.2 Multiplexed Volume Bragg Gratings

As shown in Figure 4.5, to make systems such as the one just described compact, lower their complexity and minimize the induced thermal distortions, multiplexed volume Bragg elements can be introduced. Inscribing several Bragg gratings in the same PTR glass reduces the complexity of the setup proportionally to the number of gratings recorded together. However, multiplexed VBGs are subject to inter-grating coupling effects that limit system performance. Recent studies suggested methods to overcome this limitations, paving the way to develop high-performance multiplexed devices [21].

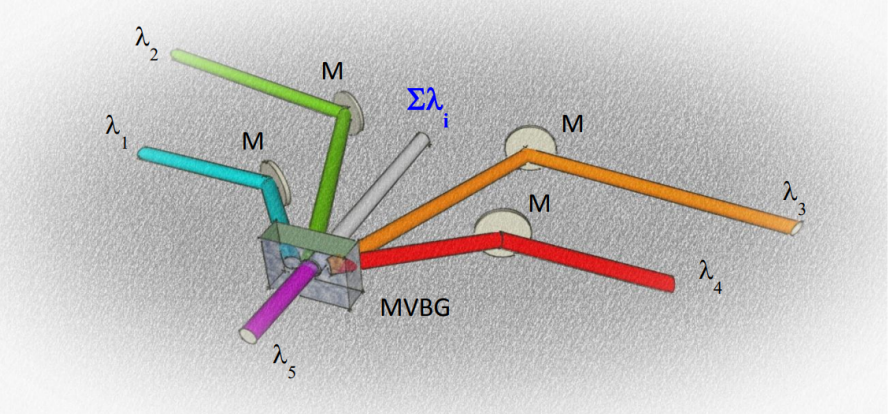

Figure 4.5: : 5-channel spectral beam combining scheme implemented by using a single reflecting MVBG.

The main drawback of an implementation that make use of volume bragg grating is the necessity to work with small angle of incidence defined with respect to the VBG's surface normal vector. As a consequence, the optical path increases and thus the occupied volume which makes such gratings not suitable for compact implementations.

4.1.3 Dichroic Mirrors

Other combining elements commonly employed in SBC are dichroic mirrors. They are usually made of thin film dielectric coatings deposited on a bulk substrate to spectrally separate incident beams by transmitting and reflecting light as a function of wavelength.

The primary benefit of employing dichroic mirrors in a combining system is their flat and large working area, which makes the alignment process significantly more straightforward.
Dichroic mirrors can be designed to function with either polarized or unpolarized light. In the case of unpolarized light, the objective of the device design is to prevent the separation of s- and p- waves and to minimize losses. This is achieved by optimizing the thickness and refractive index of the dielectric layers to ensure that the phase shift and reflectivity are wavelength-dependent, but not polarization-dependent. As a result, the dichroic mirror can effectively spectrally separate the unpolarized light without causing any significant polarization-related losses.
The angle of incidence (AOI) is typycally of 45°, however, if high powers and narrow wavelength gap are employed, the angle reduces to 22.5° in order to obtain high reflectivity and high transmittivity of the desired wavelengths for both polarizations.

Dichroic Mirrors are basically a sequence of alternated high and low quarter wave optical thickness layers (at the design wavelength) that have usually very narrow bandwidth and low absorption loss. If an equivalent transmission line model is used, the resulting equivalent reflection coefficient for normal incidence can be expressed as:

$$\Gamma_{\text{in}} = \frac{1 - \left(\frac{n_{\text{H}}}{n_{\text{L}}}\right)^{2N} \frac{n_{\text{H}}^2}{n_{\text{a}} n_{\text{b}}}}{1 - \left(\frac{n_{\text{H}}}{n_{\text{L}}}\right)^{2N} \frac{n_{\text{H}}^2}{n_{\text{a}} n_{\text{b}}}} \tag{4.1}$$

If a dichroic mirror is used to combine two different wavelength, the angle of incidence is different from 0 and the equation modifies to embody this dependency, splitting into a reflection coefficient for TE polarized and TM polarized waves. If the transmission lines theory is employed to model the cascade of bilayers, a recoursive algorithm can be used to compute the reflectivity of the dichroic mirror. Considering $M + 2$ transmission lines, where M correspond to the number of dielectric layers surrounded by an infinitely thick medium, the characteristic impedance $Z_{\infty,\text{i}}$ and the propagation constant $k_{\text{z,i}}$ have to be computed for each transmission line. As intermediate step, the Fresnel reflection coefficient is computed at each interface as:

$$\rho_{\text{i}} = \frac{Z_{\infty,\text{i}} - Z_{\infty,\text{i}-1}}{Z_{\infty,\text{i}} + Z_{\infty,\text{i}-1}} \tag{4.2}$$

Finally, proceding backwards from last interface, the refrlection coefficient seen by the wave incident on the dichroic mirror can be computed as reported in Equation 4.3

$$\Gamma_1 = \frac{\rho_{\text{h}} + \Gamma_{\text{h+1}} e^{-2jk_{\text{z,h}}L_{\text{h}}}}{1 + \rho_{\text{h}}\Gamma_{\text{h+1}} e^{-2jk_{\text{z,h}}L_{\text{h}}}}, \qquad \text{h=M,M-1,...1} \tag{4.3}$$

The typical spectrum of a dichroic mirror is reported in Figure 4.6.
It can be demonstrated that the frequency response of a dichroic mirror has a periodic behaviour. Moreover, to obtain a narrow band-rejection zone the refractive index variation between n_{H} and n_{L} should be small and the number of bilayer should be high to obtain high reflectivity and transmittivity.

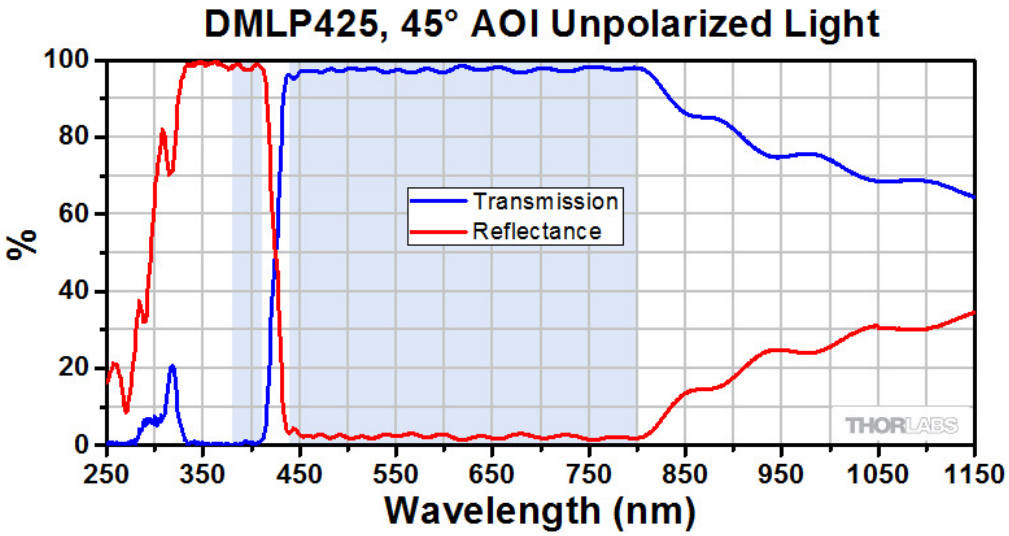

Figure 4.6: Typical spectrum of a dichroic mirror taken from Thorlabs.

Chapter 5

Spectral beam combining: Dichroic Mirror

When using dichroic mirrors for spectral combination, it is crucial to consider the impact of temperature and actual emission wavelength on the combined output. These factors can cause a non-zero linewidth and shift in the emission wavelength, which can affect the overall performance of the system.

When designing an optical system, it is crucial to consider both the typical and the min/max specifications of the devices mounted. Due to natural variation in process technology and manufacturing procedures, the emission wavelength will exhibit some amount of deviation from the ideal value. These deviations often follow Gaussian or normal distributions, and it is imperative to leverage this information to guardband the system. Moreover, temperature changes can affect the system performance both in terms of emission wavelength and dichroic spectra. Heating accounts for thermal expansion or contraction, leading to changes in the optical path length and the refractive index of the materials used in the dichroic mirror, shifting its spectra and most importantly, it causes red shift of the lasing wavelength.

In reality, each combined beam must be characterized by a different wavelength, hence the beam spectrum resulting from the spectral multiplexing will be the sum of many spectra each with a different peak wavelength. Depending on the application, the decrease of the spectral density of power may be acceptable or not. For instance, in case of fiber laser pumping applications, the absorption peak width of rare-earth doped fibers is usually of the order of 1 nm, hence the decrease of the spectral density of power severely limits the number of beams. On the contrary, in case of direct laser diode application, such as in the case of additive manufacturing, a wider spectrum is not really a concern, since what actually matters for that application is the spatial density of power and the total power carried by the laser.

Even though ideally it could be possible to combine two slightly different wavelength, the non-zero linewidth and the transition band poses some limits to this statement.

In the following sections a systematic analytical approach has been proposed to investigate the functioning of the combination technique in the absence of any statistical variation. Then, a statistical approach has been employed to assess the impact of tolerances associated with the fabrication of dichroic mirrors and multiemitter modules on the efficiency of the combining process in a practical application.

5.1 Analytical approach

To easy the simulation, 60 W multiemitter module are assumed to be composed of 16 CoC emitting at the same wavelength λ_{pk}, different for each module.
The above mentioned assumption is not overly restrictive for analysis purposes. This is due to the fact that in actual multi-emitter modules, the CoC units are carefully tested and selected based on the desired emission wavelength. As a result, the final output spectra of the module is typically very similar to that of the individual CoC units.
The selection process involves rigorous testing and quality control measures to ensure that the CoC units meet the required specifications for the module. This may include measures such as wavelength sorting and binning, as well as adjustments to the operating conditions of the CoC units to ensure that they emit at the desired wavelength.
Therefore, while the assumption of identical emission wavelength for all CoC units in a multi-emitter module may not hold strictly true in practice, the careful selection and testing of the individual units ensures that the output spectra of the module closely approximates that of the individual CoC units.

The combination via Dichroic Mirror of the aforementioned modules is analyzed in the following scenarios:

- non stabilized modules combination via ideal dichroic mirror;
- non stabilized modules combination via real dichroic mirror both without considering manufacturing tolerances and simulating the worst case of manufacturing tolerances;
- VBG stabilized modules combination via ideal dichroic mirror. As a first step, the red shift due to VBG heating is neglected;
- VBG stabilized modules combination via real dichroic mirror considering worst case manufacturing tolerances and temperature shift;
- Optimized non stabilized modules combination via real dichroic mirror.

The modeled ideal dichroic mirror spectrum is represented by a piecewise linear function characterized by a transmission flat band and a reflection flat band with in between

a transition band that for simplicity is assumed to be a straight line.

$$T_{\mathrm{DM}} = \begin{cases} 0 & \text{if} \quad \lambda - \lambda_{\mathrm{DM}} \leq -\Delta\lambda_{\mathrm{DM}}/2 \\ \lambda - \lambda_{\mathrm{DM}} & \text{if} \quad -\Delta\lambda_{\mathrm{DM}}/2 \leq \lambda - \lambda_{\mathrm{DM}} \leq \Delta\lambda_{\mathrm{DM}}/2 \\ 1 & \text{if} \quad \lambda - \lambda_{\mathrm{DM}} \leq \Delta\lambda_{\mathrm{DM}}/2 \end{cases} \tag{5.1}$$

The obtained ideal spectrum is reported in Figure 5.1.

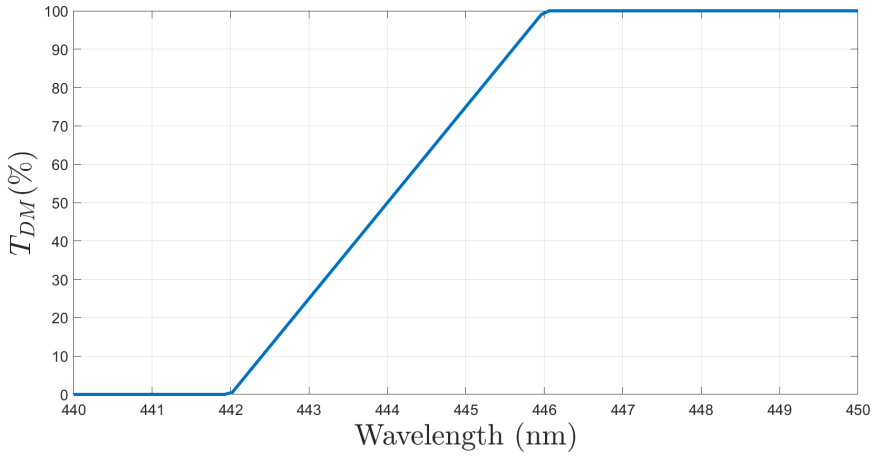

Figure 5.1: Ideal Dichroic Mirror spectrum.

If a more realistic spectrum is desired, the equivalent transmission model should be employed, and a proper optimization should be performed. The reflectivity of a dichroic mirror at oblique angles of incidence (AOI) can vary for s- and p-polarized waves. To avoid significant losses due to this polarization-dependent reflectivity, the refractive index and the number of bilayers in the mirror are carefully designed. The design process typically involves numerical simulations and optimization algorithms to find the optimal combination of layer thicknesses and refractive indices. This allows for the development of dichroic mirrors that are highly efficient and can meet the specific requirements of a given application.

A more realistic dichroic mirror spectrum is reported in Figure 5.2, where the high refractive index is fixed for each bilayer while the low refracrive index varies in between each layer, in order to reduce side lobes in the stop band of the spectral response.

Supposing each multi-emitter is comprised of 2N Chip on Carrier blue laser diodes, with the first N devices emitting at a typical emission wavelength of 442 nm and the remaining N devices emitting at 448 nm, both minimum and maximum emission wavelength falling within the range specified in commercial diode laser's datasheet, a Cauchy distribution has been assumed for the spectral density of power of each beam to better model the characteristic long tails of High Power Laser Diodes spectra:

$$\frac{\partial P}{\partial \lambda}(\lambda; \lambda_{\mathrm{pk}}, \gamma) = \frac{A\gamma^2}{\pi\gamma((\lambda - \lambda_{\mathrm{pk}})^2 + \gamma^2)} \tag{5.2}$$

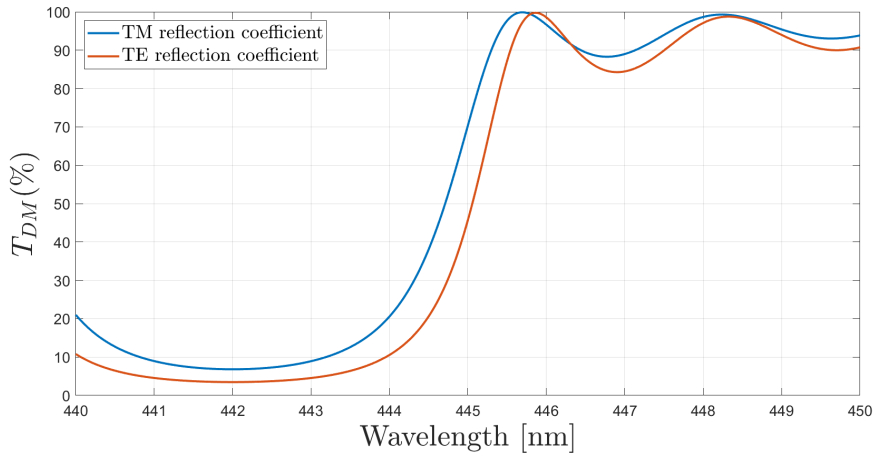

Figure 5.2: Transmission spectrum of a dichroic mirror working at AOI 22.5°.

where A is a constant such that the cumulative power is normalized; γ is the full width half maximum of the spectral distribution; λ_{pk} is the emitting peak wavelength. The amount of power the i-th laser diode delivers, once it has passed through the dichroic mirror is equal to

$$P_{\mathrm{i}}^{del}(\lambda_{\mathrm{pk}}^{i}(T), \Delta\lambda_{\mathrm{DM}}) = \int d\lambda \frac{\partial P}{\partial \lambda}(\lambda; \lambda_{\mathrm{pk}}, \gamma) U_{\mathrm{DM}}^{i}(\lambda; \lambda_{\mathrm{DM}}, \Delta\lambda_{\mathrm{DM}}) \tag{5.3}$$

where

$$U_{\mathrm{DM}}^{i}(\lambda_{\mathrm{DM}}, \Delta\lambda_{\mathrm{DM}}) = \begin{cases} T_{\mathrm{DM}}(\lambda; \lambda_{\mathrm{DM}}, \Delta\lambda_{\mathrm{DM}}) & \text{if} \quad 1 \leq i \leq N \\ 1 - T_{\mathrm{DM}}(\lambda; \lambda_{\mathrm{DM}}, \Delta\lambda_{\mathrm{DM}}) & \text{if} \quad N+1 \leq i \leq 2N \end{cases} \tag{5.4}$$

The total output power, for a single realization of the system is given by:

$$P_{\mathrm{DM}}^{tot}(\{\lambda_{\mathrm{pk}}(T)\}_{\mathrm{r}}, \Delta\lambda_{\mathrm{DM}}) = \sum_{\mathrm{i}=1}^{2N} P_{\mathrm{i}}^{del}(\lambda_{\mathrm{pk}}^{i}(T), \Delta\lambda_{\mathrm{DM}}) \tag{5.5}$$

and the system efficiency can be expressed as:

$$\eta_{\mathrm{DM}}(\lambda_{\mathrm{pk}}^{i}(T), \Delta\lambda_{\mathrm{DM}}) = \frac{P_{\mathrm{DM}}^{tot}(\{\lambda_{\mathrm{pk}}(T)\}_{\mathrm{r}}, \Delta\lambda_{\mathrm{DM}})}{2NP_0} \tag{5.6}$$

where P_0 is the total power emitted by each emitter.

Simulation of two 60 W multi-emitter modules combination via dichroic mirror is reported in Figure 5.3, where efficiency versus driving current is reported. Assuming that each multi-emitter is composed of two polarization combined stacks of 8 CoC, with a typical polarization purity higher than 90%, the module output can be represented as a combination of s-polarized waves and p-polarized waves, each contributing 50% of the total power.

Since the module output is directed towards a dichroic mirror, which reflects light based on its polarization, each polarization component will be affected by the reflectivity of the dichroic mirror calculated for its specific polarization. Thus, the s-polarized wave component will be reflected by the mirror with an efficiency determined by the reflectivity of the mirror for s-polarized waves, while the p-polarized wave component will be reflected by the mirror with an efficiency determined by the reflectivity of the mirror for p-polarized waves.
Finally, by summing the contributions of the s-polarized and p-polarized components after their respective reflections, the overall output of the module is obtained and reported in Figure 5.3.

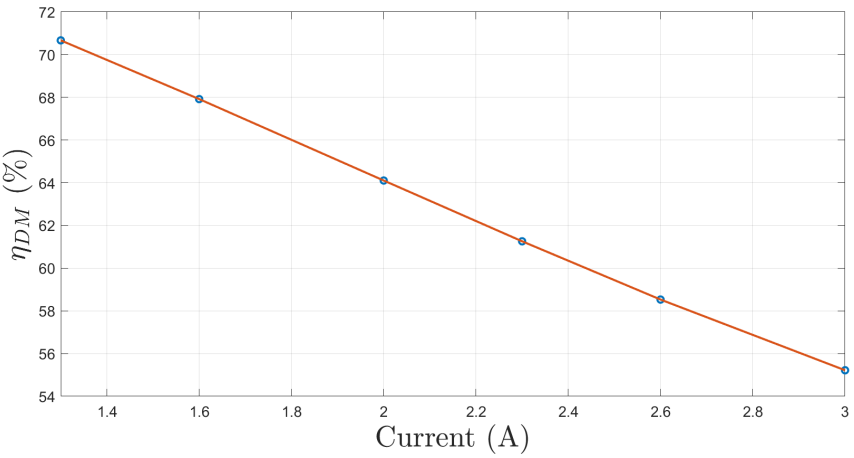

Figure 5.3: Combining efficiency of non stabilized modules with a red shift of $1.3\,\mathrm{nm\,A^{-1}}$.

As it can be clearly deduced, there is no advantage of spectral combination if the emission wavelength of the incident beams that should be transmitted and reflected are not fixed in the flat band of respectively the transmission and reflection zone.

If tolerances in dichroic fabrication are introduced, the situation worsens significantly. Figure 5.5 and Figure 5.4 depict the TM and TE transmission curves, respectively, for a +/-1% uncertainty in the thickness of each bilayer, simulating in such way the worst case scenario. The resulting efficiency curves versus current for the combining system are simulated and illustrated in the accompanying Figure 5.6.
Due to the high variation of efficiency, combination without locking of the emission wavelength is hardly feasibile.

To overcome this issue, stabilization is conducted and its simulation is outlined in the following paragraph. In particular, for the considered dichroic, the transition between the reflected and transmitted band is of almost 4 nm, therefore stabilization via Volume Bragg Gratings is simulated in Figure 5.7, Figure 5.8 and Figure 5.9 with the following characteristics:

- The emission wavelength for the transmitted beam is fixed at 448 nm and for the

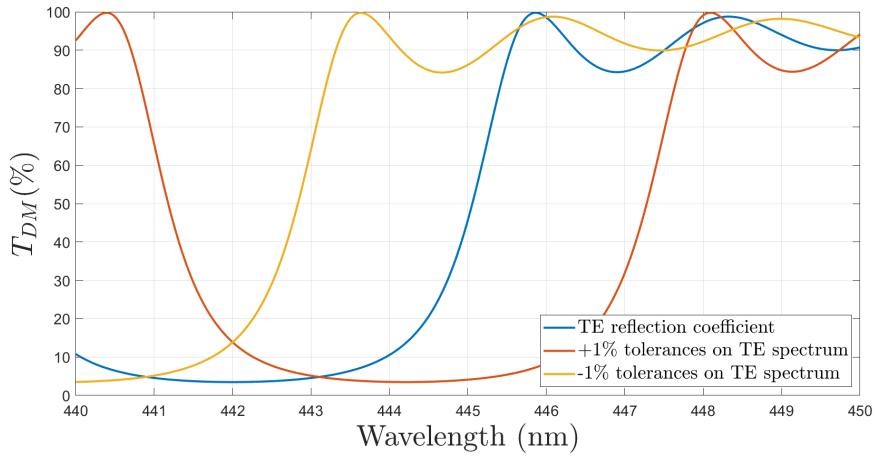

Figure 5.4: Dichroic spetra for TE polarized waves with +1% and -1% tolerances in the thickness of each bilayer.

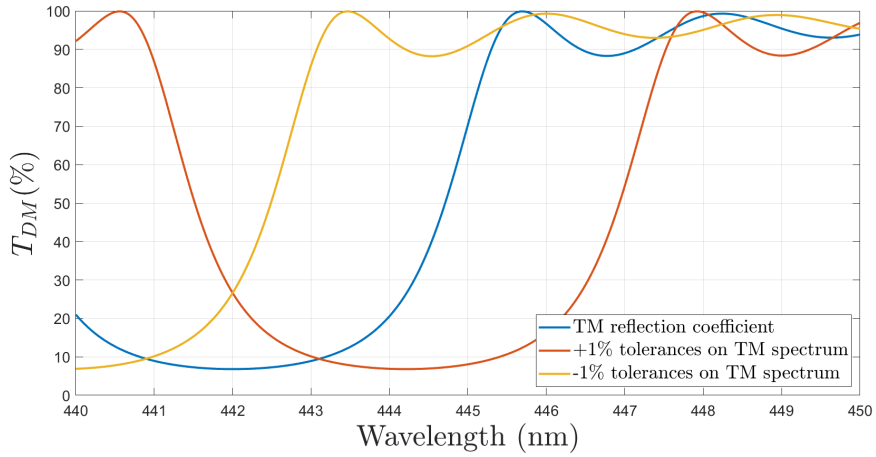

Figure 5.5: Dichroic spetra for TM polarized waves with +1% and -1% tolerances in the thickness of each bilayer.

reflected beam is fixed at 442 nm by the VBGs;

- the FWHM is extrapolated from datasheet of commercial VBGs and it is fixed at 0.1 nm;
- thermal shift due to increased driving current is neglected. This is because experimental measurements have shown that the magnitude of this shift is typically only on the order of a fraction of nm and therefore does not significantly impact the overall performance of the system.

The total combining efficiency drop due to the introduction of manufacturing tolerances is around 12%, which is almost half the drop expected for non stabilized modules.

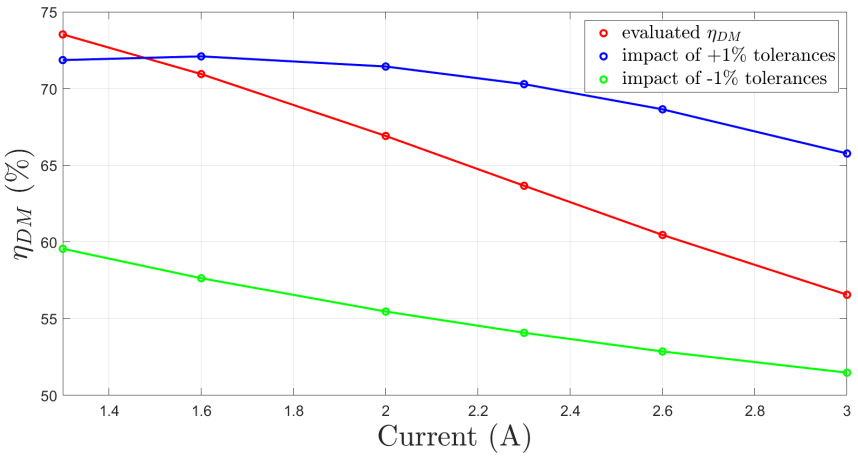

Figure 5.6: Efficiency drop due to current increase including tolerances.

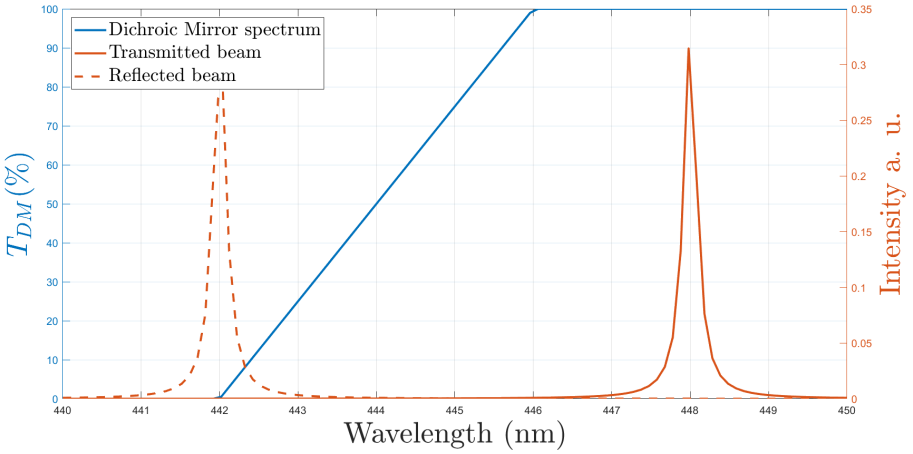

Figure 5.7: Spectral behaviour of the normalized reflected and transmitted beam. The dichroic mirror behaviour is reported in blue.

Moreover, no shift of wavelength is expected due to driving current, assuring a constant response regardless of the operational current.

In order to better appreciate the importance of locking the laser diode emission wavelength, the impact of thermal shift is introduced. When temperature rises, the peak wavelength of HPLDs shifts towards longer wavelengths; moreover, their spectral full width at half maximum increases too even though it is not modeled for simplicity. However, the presence of Volume Bragg Gratings strongly reduces the impact of temperature for variation ranges of tens of Celsius due to the small ρ_T that has been experimentally evaluated to be equal to $5\,\mathrm{pm}\,^{\circ}\mathrm{C}^{-1}$ from the plot reported in chapter 3. The dependecy

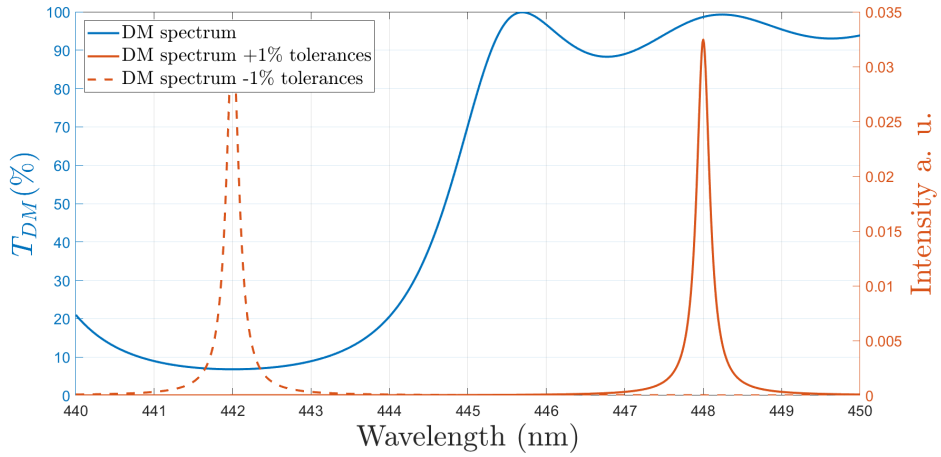

Figure 5.8: Spectral behaviour of the normalized reflected and transmitted beam. The dichroic mirror behaviour is reported in blue.

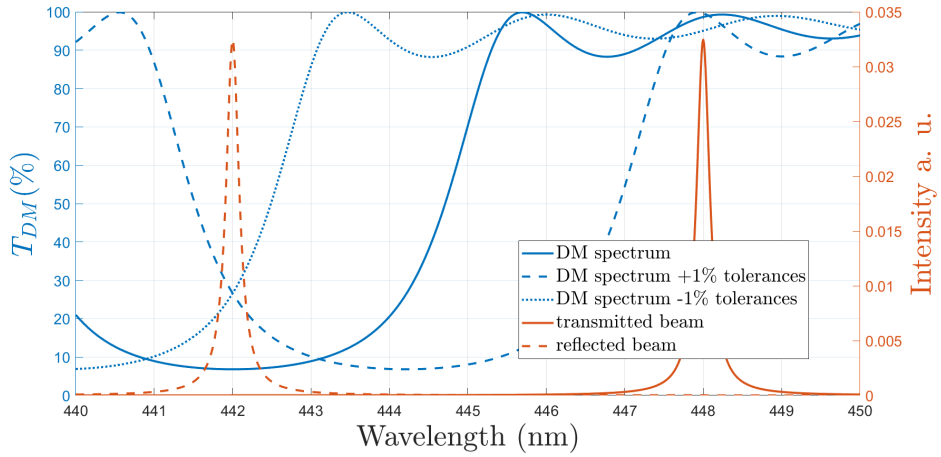

Figure 5.9: Spectral behaviour of the normalized reflected and transmitted beam. The dichroic mirror behaviour is reported in blue. For simplicity only the TM polarized wave DM spectrum is reported.

simulated is:

$$\lambda_{\mathrm{pk}} = \lambda_{\mathrm{VBG}} + \rho_{\mathrm{T}}(T - T_0) \tag{5.7}$$

where λ_{VBG} is the central wavelength of the VBG at $T = T_0$, T is the temperature and ρ_{T} is a proportional constant that takes into account the wavelength drift due to temperature changes extrapolated from experimental measurements. The Dichroic Mirror response is supposed to be not dependent on temperature because its shift due to temperature is in general an order of magnitude smaller than the shift with respect to the temperature of the peak wavelengths, thus it is neglected.
The combining efficiency variation in the temperature range 20 °C ÷ 40 °C is plotted in

Figure 5.10 proving the feasibility of spectral combination via Dichroic Mirror of stabilized emission spectra by means of Volume Bragg Gratings.

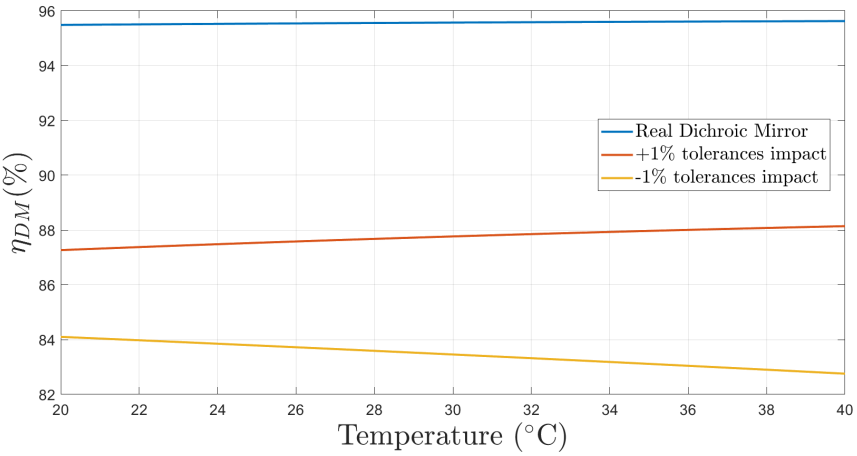

Figure 5.10: Combining efficiency vs temperature of stabilized multi-emitters.

In Table 5.1 all combining efficiencies are gathered together to better appreciate the advantage of stabilization prior spectral combination.

	ideal DM	real DM	worst case tolerances real DM
non stabilized	$\bar{\eta} = 62.95\%$, $\sigma = 5.79\%$	$\bar{\eta} = 65.34\%$, $\sigma = 6.4\%$	$\bar{\eta} = 55.18\%$, $\sigma = 3.02\%$
stabilized	$\eta = 98.02\%$	$\eta = 95.44\%$	$\eta = 85.23\%$

Table 5.1: Comparison between the averaged (over the current range) combining efficiency of a non stabilized system and a stabilized system with different dichroic mirror realizations and working condition.

In situations where power scaling is used to achieve the highest possible output power in all applications, and modulation is not a concern, the design of spectral combination must be reviewed to optimize the transition band. This is done to ensure that the transition band falls between the transmitted and reflected wavelengths at the maximum current. It is important to note that the maximum wavelength could vary from the typical one stated in the datasheet due to temperature drift. As a result, careful consideration must be given to optimizing the transition band to achieve the desired output power.

In the following section, the evaluation of combining efficiency is performed directly for a realistic dichroic mirror considering both no tolerances in the manufacturing and introducing +/-1% tolerances in each layer of the dichroic fabrication.

In Figure 5.11 efficiency curves at 3 A driving current are plotted with respect to

temperature increase, and in Table 5.2 the efficiency are compared with the stabilized module combination.

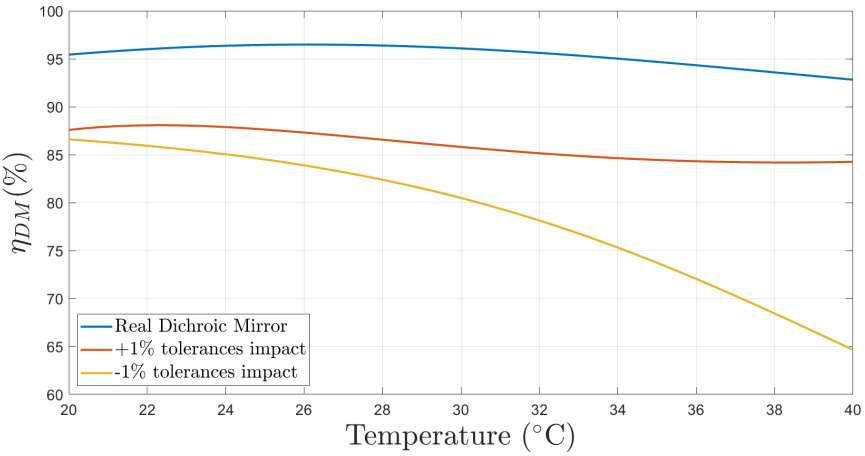

Figure 5.11: Combining efficiency of two 60 W non stabilized modules spectrally combined by means of a realistic dichroic with and without considering the impact of tolerances.

Table 5.2: Comparison between the combining efficiency of a stabilized and a non stabilized system with different dichroic mirror realizations and working condition at fixed operational current.

	realistic DM	max drop due to +/-1% tolerances	max drop due to T
non stabilized	95.43%	8.83%	21.94%
stabilized	98.02%	2.58%	1.13%

5.2 Statistical approach

The multi-emitter module employed for stabilization purposes in chapter 3 exhibits a deficiency in terms of wavelength sorting and binning. Consequently, the spectra acquired from this module is comprised of n-CoC, each of which emits at a unique wavelength within the range of 442 nm ÷ 446 nm. This particular condition significantly constrains the process of spectral combination, and the influence of this production technique is integrated into the subsequent statistical methodology.

The following assumption are made:

- Two 60 W modules made of two stack of 8 CoC polarization combined each emitting at 4 W are spectrally combined;
- the emission wavelength of each chip has a Gaussian probability distribution centered at 444 nm with a standard deviation of 0.25 nm;

- each dichroic has been realized with a random tolerance in the range ±2% in absolute value

The initial simulation has been conducted 1000 times, with each iteration involving the extraction of the emission wavelength of each chip from its respective Gaussian distribution. Additionally, the simulation evaluate the combining efficiency, given the dichroic mirror spectrum displayed in Figure 5.2. A representative spectrum, obtained from one of the simulations performed, is reported in Figure 5.13. A close inspection of the spectrum reveals the characteristic features of a multi-emitter configuration, wherein the CoC exhibit a variation in their actual emission wavelength. Consequently, this leads to a broadening of the spectral distribution and a deviation from a perfect bell shape.

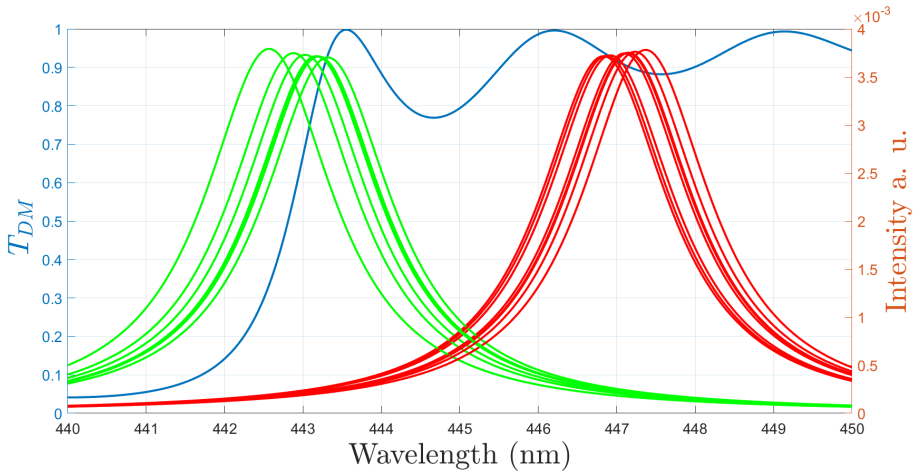

Figure 5.12: Spectrum measurement of a real dichroic mirror realization (blue) and spectrum of the transmitted (green) and reflected (red) CoC spectrum composing the multi-emitter.

The combining efficiency calculated with and without including fabrication tolerances is reported in Figure 5.15 where mean values and standard deviations are reported for the specified driving currents.
The dichroic mirror transmission spectra considered are reported in Figure 5.14 and are obtained by randomly adding a fabrication tolerance in the range of +1% and -1% different for each layer.

For comparison purpose, in Table 5.3 combining efficiency at maximum driving currents are reported for both stabilized and non stabilized modules in all the mentioned combination. The stabilized combining efficiency without DM tolerances is not characterized by a mean and a standard deviation because the emission wavelength is supposed deterministic and fixed by the VBG peak wavelength.

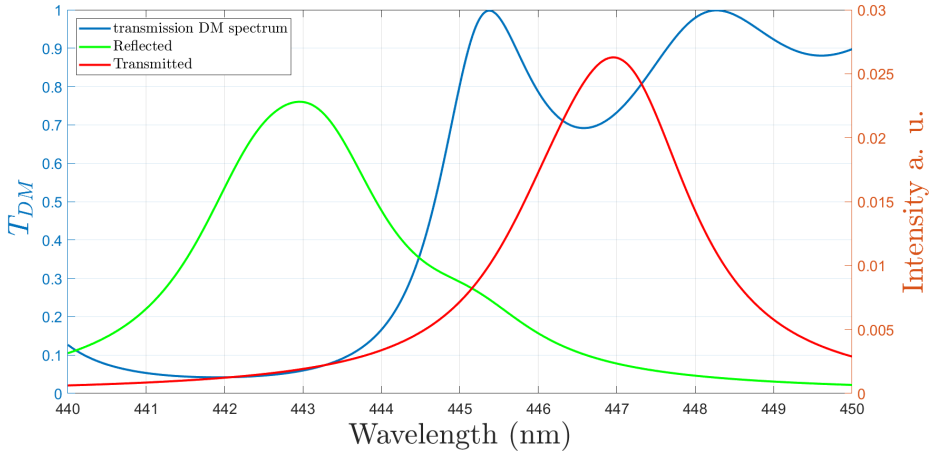

Figure 5.13: Spectrum measurement of a real dichroic mirror realization (blue) and spectrum of the transmitted (green) and reflected (red) module spectrum.

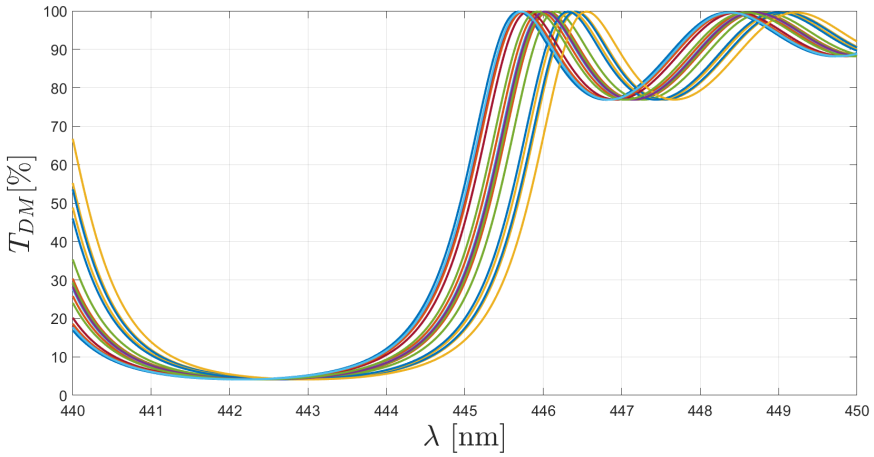

Figure 5.14: Collection of transmissivity curves, from which the spectrum of the dichroic mirror is selected for each iteration. The set of represented curves is reduced to easy the representation.

Table 5.3: Comparison between the combining efficiency of a stabilized and a non stabilized without wavelength selection module system with different dichroic mirror realizations and working condition at fixed operational current (3 A).

	without DM tolerances	considering DM tolerances	max drop due to T
non stabilized	$\bar{\eta} = 65.13\%$, $\sigma = 1.88$	$\bar{\eta} = 79.62\%$, $\sigma = 1.12$	$\bar{\eta}_{\text{drop}} = 15.32\%$, $\sigma = 1.83$
stabilized	$\eta = 98.02\%$	$\bar{\eta} = 95.44\%$	$\bar{\eta}_{\text{drop}} = 1.13\%$

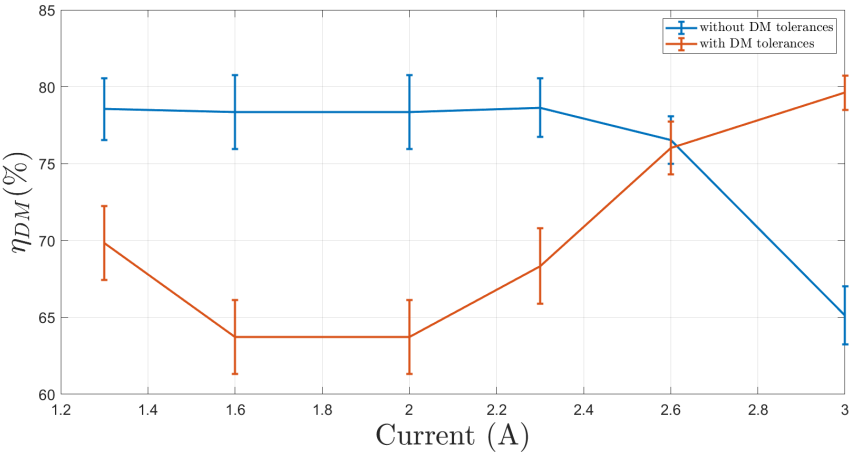

Figure 5.15: Plot of the combining efficiency calculated at different driving currents with and without considering dichroic mirror tolerances.

Chapter 6

Prototype Design

6.1 Zemax OpticStudio

To design the optical system and prove the expected behaviour, OpticStudio software from Zemax has been used, and in particular *Non-sequential* mode.

Non-sequential ray tracing does not involve a predetermined order of surface interactions between traced rays. The path of a ray is solely determined by the physical properties and spatial locations of the objects encountered, as well as the direction of the ray itself. Thus, a ray may intersect any part of a non-sequential object, and may potentially encounter the same object multiple times or not at all.

In the context of Non-Sequential Mode, optical components are represented as true three-dimensional objects, which can be either surface or solid volumes. Each object is assigned a unique global position with independent x, y, z coordinates and an orientation that is independently defined.

When using pure non-sequential ray tracing, *source* and *detector* objects are available to launch and record rays, respectively. Sources can be placed anywhere in the non-sequential group, at any orientation and can range from simple point sources to complex, three-dimensional source distributions.

Rays from non-sequential sources, known as *NSC rays*, can be split and scattered by optical components. These rays can also be diffracted at phase surfaces/objects. The analysis options available when tracing NSC rays include evaluating radiometric data on detectors and the storing of ray data in ray database files. Detectors can be modeled as planar surfaces, curved surfaces, and even three-dimensional volumes.

For the evaluation of performance the following assumptions are made:

- Sources are modeled to resemble the emission of the multi-emitters employed for the final prototype;

- VBGs are not simulated, instead precise locking at the Bragg wavelength is assumed for each source;
- The Broadband dielectric Mirror has been imported from Thorlabs and coating -E02 has been added;
- To model the dichroic coating, table coating option is used because it allows the transmission, reflection, and absorption properties of a coating to be wavelength, polarization, and angle of incidence dependent.

6.1.1 Source

A real laser diode stack based on Zemax ray tracing software that operates in a non-sequential mode is reported. The module used in the prototype is characterized by the beam characteristics illustrated in fig. 6.1.

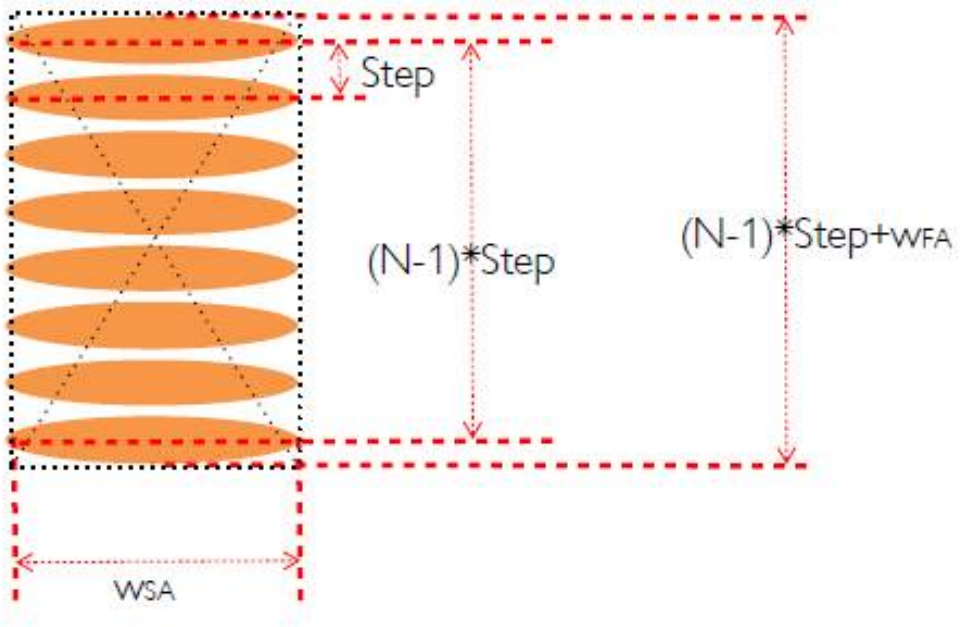

Figure 6.1: Output characteristic of Convergent multi-emitters modules.

For this purpose, two Source Diode sources are used and superimposed to simulate spectral combination. Each of these sources is comprised of 8 stacked virtual diodes, vertically spaced by a *Step* parameter of 0.4 mm and with divergence $\theta_{\mathrm{SA}} = 1.87\,\mathrm{mrad}$ and $\theta_{\mathrm{FA}} = 1.93\,\mathrm{mrad}$.

Since each diode is simulated as a point source, the *Astigmatism* parameter of the Source Diode has been calculated as explained in Eq. 6.1 in order to obtain the simulated beam waist diameter on the SA $w_{\mathrm{SA}} = 2.15\,\mathrm{mm}$ and the source has been shifted by $-69.5\,\mathrm{mm}$ in the negative z-axis direction in such a way as to obtain a FA beam waist diameter $w_{\mathrm{FA}} = 0.27\,\mathrm{mm}$ at position $z = 0$.

$$Astigmatism = \frac{w_{\mathrm{SA}}}{2\tan\theta_{\mathrm{SA}}} = 574.9\,\mathrm{mm} \tag{6.1}$$

The field distribution of the simulated source obtained with the parameters just explained is shown in Figure 6.2.

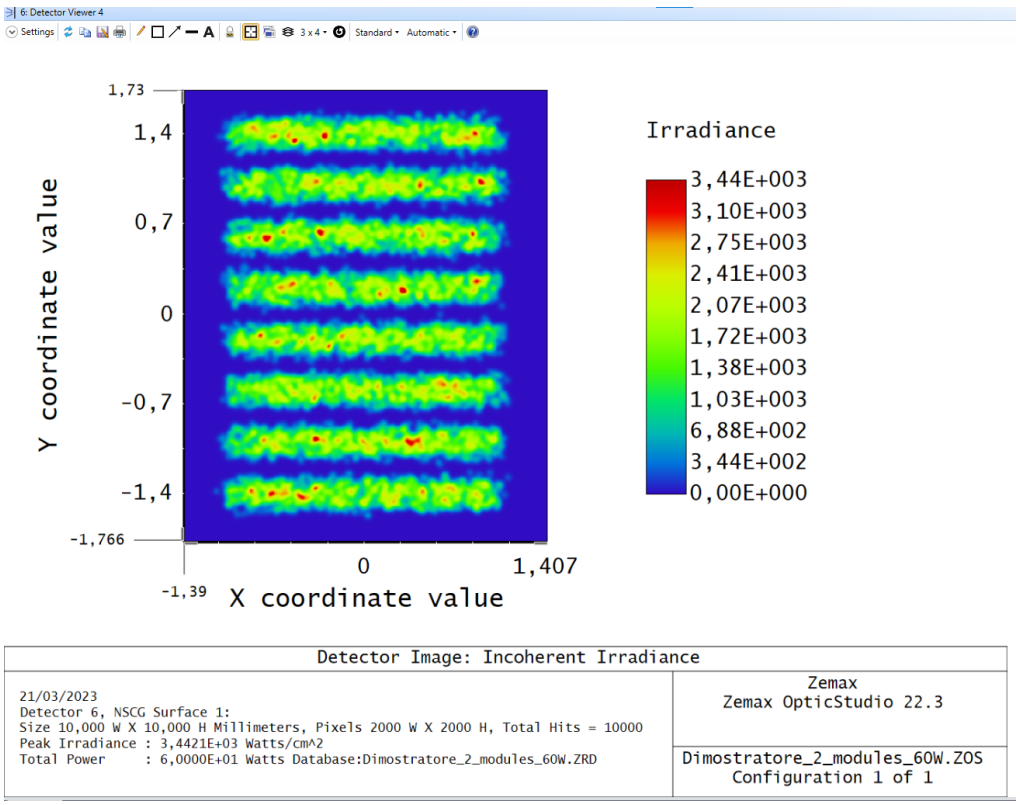

Figure 6.2: Spot diagram of the simulated 60W multi-emitter source.

6.1.2 Dichroic Coating

For table coatings, data is normally specified at multiple angles of incidence. At each angle of incidence specified, the polarization dependent reflection and transmission for several wavelengths is specified. The syntax for table coatings is the following:

```
   TABLE [coating name]
ANGL [angle of incidence 1, in degrees]
WAVE [wavelength 1, in mm] [Rs] [Rp] [Ts] [Tp] [Ars] [Arp] [Ats] [Atp]
WAVE [wavelength 2, in mm] [Rs] [Rp] [Ts] [Tp] [Ars] [Arp] [Ats] [Atp]
```

where R_{s} and R_{p} are the reflection coefficient of s and p polarized wave and T_{s} and T_{p} are the transmission coefficient. The remaining parameters are the phase rotation angles.

If the angles are omitted, no phase change will be introduced by the coating.

The coating introduced is reported in Figure 6.3 and it has the same behaviour of the piecewise linear function described in MATLAB. It has not been described a more realistic coating due to the limitations imposed by the software simulator that does not allow simulation of complex emission spectrum.

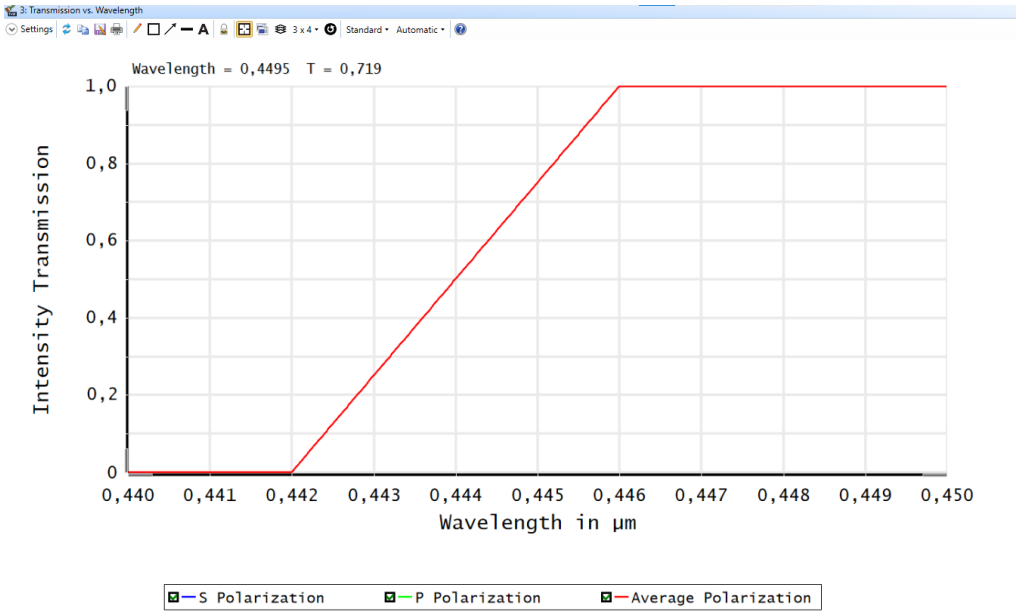

Figure 6.3: Transmission vs Wavelength plot of the Dichroic coating simulated in Zemax OpticStudio.

6.1.3 Combined output

The result of the superposition of two sources is represented in Figure 6.5 and refers to the schematic of Figure 6.4 where one mirror placed at 22.5° is used to drive the emission of the module on one side of the dichroic mirror with AOI 22.5°.

The power delivered after the first dielectric mirror is 59.40 W, 99% of the input optical power. The remaining 0.01% is lost due to the E02 Thorlabs coating.

The total output power after spectral combination is of 119.4 W. The simulation performed doesn't take into account the non zero linewidth of the laser. However, it proves the feasibility of spectral combination as a power scaling method capable of almost doubling brightness while keeping the same beam quality.

The above mentioned schematic could be considered as the building block of a scalable source, capable of scaling without any reconfiguration. Nevertheless, it is important to note that the design is subject to critical limitations posed by the dichroic mirror. Specifically, the minimum transition band of the dichroic mirror cannot be less than

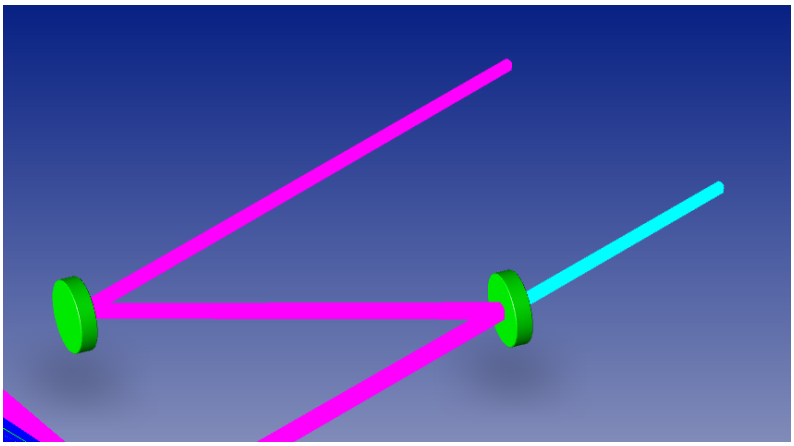

Figure 6.4: Set up simulated in OpticStudio to spectrally combine two modules.

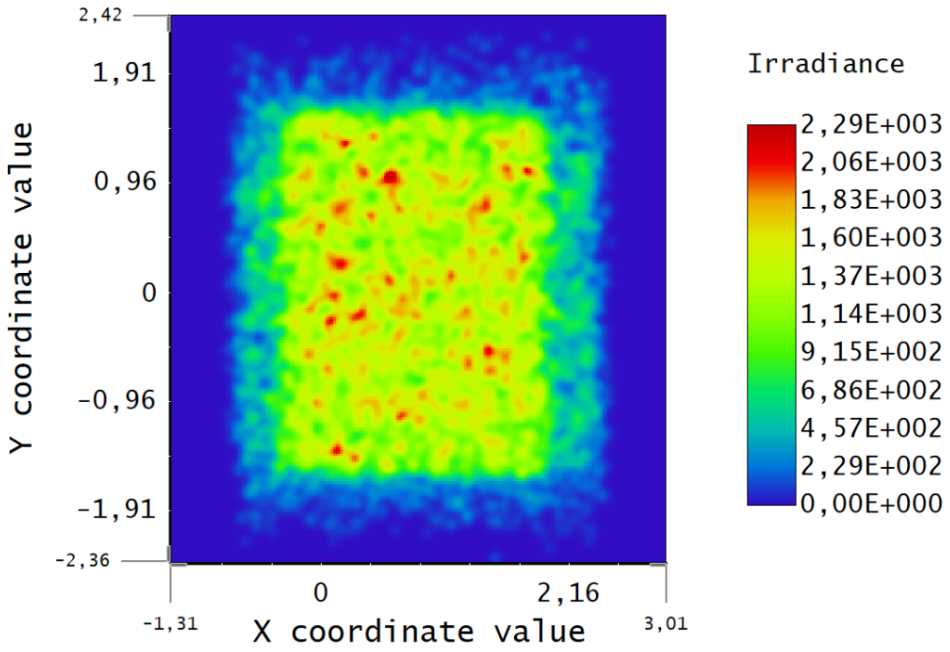

Figure 6.5: Spot diagram of the superposition of the two simulated sources spectrally combined.

4 nm, as it stands with current technology. This poses a significant challenge for the design of the source and must be taken into account during the development process.

6.1.4 Spatial combination

To further increase the output power without introducing excessive complexity and while maintaining cost-effectiveness, an intermediate step of spatial combination has been implemented to effectively merge two pairs of spectrally combined modules.

This approach offers the benefit of low costs since it employs the same specific combining element without requiring any redesign or modifications, which can be produced on the same wafer. Additionally, a prism with the appropriate facet coating serves as the spatial combining element that can rotate and merge beams that would otherwise be impossible to combine due to the mechanical limitations of the optical component and module themselves. This solution can be easily ordered without the need for a custom design. It should be noted, however, that this approach sacrifices beam quality and brightness due to the combining technique.

If an all-spectral combination is pursued, the beam quality can be maintained, but the design would require a more expensive and complex dichroic element that can combine four wavelengths within the range of 440 nm ÷ 455 nm, which are respectively the minimum and maximum emission wavelengths specified in the commercial CoC datasheet. It should be emphasized that finding multi-emitters with sufficient gain to lase at the limit of GaN bandwidth is not a trivial task.

The proposed configuration is illustrated in Figure 6.6, and the resulting beam spot is depicted in Figure 6.7. As can be observed, the beams are merged but not perfectly superimposed. Nevertheless, the superimposition is achieved in the focal plane by incorporating a processing head that is specifically designed for this purpose. It should be noted that the details of this processing head are beyond the scope of this work and will not be discussed further.

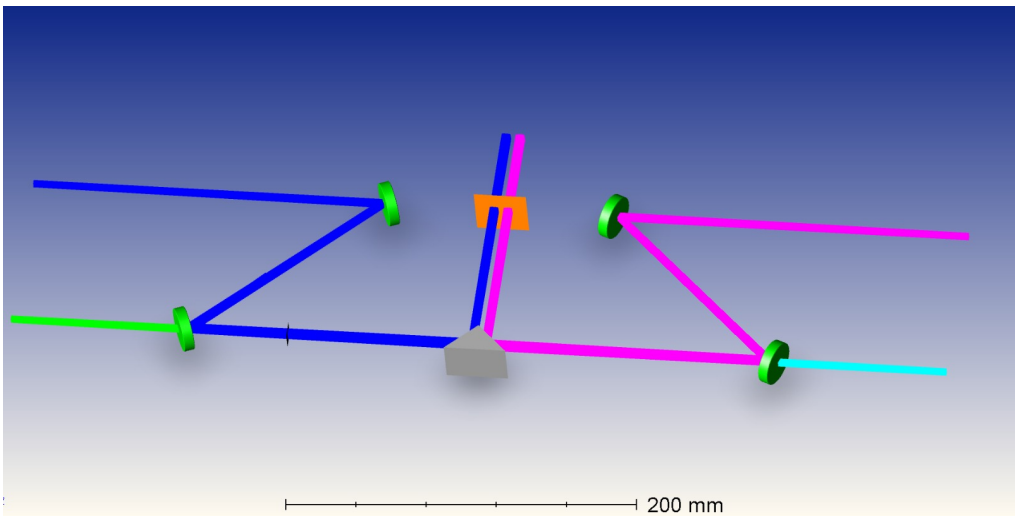

Figure 6.6: Set up for spatial combination of spectrally stabilized modules.

Furthermore, this design offers the possibility of achieving a compact and scalable solution in which up to 8 modules could be combined without requiring any reconfiguration or redesign of the optical components. This feature represents a significant advantage as it allows for a flexible and easily expandable system, with the potential to meet changing

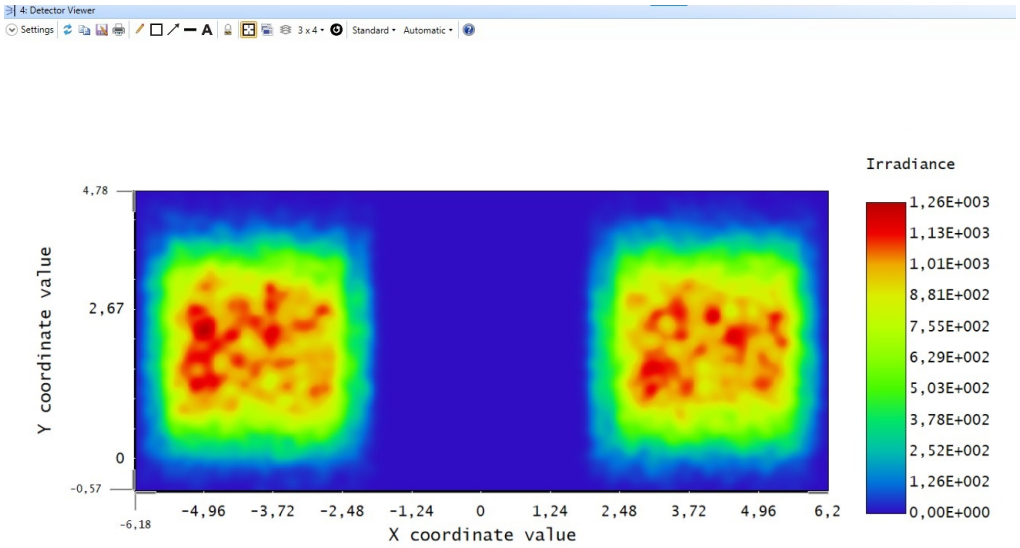

Figure 6.7: Spot of the spatial combined modules.

demands in the future.

Chapter 7

Conclusions

In conclusion, this master thesis has investigated the potential of spectral combination of blue multi-emitter modules and their stabilization via Bragg gratings. The study has revealed that this approach has great promise for the development of high-power, high-brightness blue laser sources that are cost-effective and simple to implement. However, the minimum transition band of the dichroic mirror poses a critical limitation on the design, and the use of spatial combination has been explored as a solution to further increase power while keeping costs under control.

In chapter 1 a brief overview of Laser Additive Manufacturing is given, market trends are reported emphasizing how Metal AM demand is forecast to increase in the next five years. In terms of laser type, solid-state laser segment seems to dominate the market during the forecast period due to their light weight, small size and compactness. Finally, a brief overview of laser sources and laser parameters influencing AM is mentioned. Blue laser light is remarked to be the best choice for metal AM due to their high absorption with respect to standard IR and CO2 lasers.
The basics of power scaling are illustrated in chapter 2, where spatial and polarization multiplexing are briefly discussed to explain multi-emitter structure. Spectral beam combining and coherent beam combining technique are compared. In conclusion, wavelength multiplexing appears to be the best solution in terms of costs, scalability and reliability. In chapter 3, experimental results performed on the stabilized 30 W multi-emitter module showed good performance over all the current and temperature range of operation. The findings have shown that Bragg gratings are an effective means of stabilizing the output spectrum, improving the performance of the laser source, and controlling temperature and current drifts. The above mentioned results are expected to hold for the 60 W module to be mounted on the prototype because made of polarization combination of two 30 W modules. Moreover, temperature analysis has been adjusted to met the working wavelength and it is possible to predict VBG heating.

The spectral beam combining has been fully introduced in chapter 4 and theoretically analyzed in chapter 5 where both an analytical and a statistical approach are proposed to estimate spectral combining efficiency and the expected optical output power. The

conducted studies emphasize the importance of stabilization prior combining.

Finally, in chapter 6, the prototype architecture is illustrated and ray tracing analysis is performed in OpticStudio. The adoption of a software tool for ray tracing is justified by the complex source that cannot be modeled properly by means of Gaussian beams due to the high M2 value.

Overall, the results of this study have contributed to the development of a scalable and reliable blue laser source for various applications, particularly for laser additive manufacturing where spectral purity is not crucial. Future research should focus on overcoming the limitations posed by the dichroic mirror and optimizing the design for specific applications.

Overall, the results of this study have contributed to the development of a scalable and reliable blue laser source for various applications, particularly for the next generation of laser-based AM machines. Future activities will have to be focused on the optimization of the designed source once the experimental data of its implementation will be available. Moreover, further investigations in the field of material processing are necessary to properly design the source starting from the specification of power and required brightness.

Bibliography

[1] G. Pedroza, L. Bechou, Y. Ousten, L. S. How, O. Gilard, J.-L. Goudard, and F. Laruelle, "Long term in-vacuum reliability testing of 980nm laser diode pump modules for space applications," pp. 1–14, 03 2014.

[2] H. Kissel, J. W. Tomm, B. Koehler, and J. Biesenbach, "Impact of external optical feedback on high-power diode laser lifetime and failure modes," in *HIGH-POWER DIODE LASER TECHNOLOGY XVII* (M. Zediker, ed.), vol. 10900 of *Proceedings of SPIE*, SPIE, 2019. Conference on High-Power Diode Laser Technology XVII, San Francisco, CA, FEB 03-05, 2019.

[3] A. S. Chernikov, R. V. Chkalov, and D. G. Vasilchenkova, "Volume bragg grating fabrication by femtosecond laser pulses," in *2020 International Conference Laser Optics (ICLO)*, pp. 1–1, 2020.

[4] "Additive manufacturing, general principles, fundamentals and vocabulary," p. 14, ASTM, 2021.

[5] "Global laser technology market revenue analysis and forecast." www.acumenresearchandconsulting.com/.

[6] "Laser technology market size - global industry, share, analysis, trends and forecast 2022 - 2030," p. 250, IEEE, 2022.

[7] L. Li, "The advances and characteristics of high-power diode laser materials processing," *Optics and Lasers in Engineering*, vol. 34, no. 4, pp. 231–253, 2000. Laser Material Processing.

[8] Y. Xiong, C.-l. Jiang, A. Jamil, X. Liu, X. Liu, P. Modak, S. McDougall, and K. Boucke, "Advances in 976nm single emitter broad semiconductor diode lasers for 300w+fiber laser pump module applications," in *HIGH-POWER DIODE LASER TECHNOLOGY XX* (M. Zediker and E. Zucker, eds.), vol. 11983 of *Proceedings of SPIE*, SPIE, 2022. Conference on High-Power Diode Laser Technology XX at SPIE LASE Conference, ELECTR NETWORK, JAN 22-FEB 28, 2022.

[9] J. Piprek, "What limits the power conversion efficiency of gan-based lasers?," in *PHYSICS AND SIMULATION OF OPTOELECTRONIC DEVICES XXV* (B. Witzigmann, M. Osinski, and Y. Arakawa, eds.), vol. 10098 of *Proceedings of SPIE*, SPIE, 2017. Conference on Physics and Simulation of Optoelectronic Devices XXV, San Francisco, CA, JAN 30-FEB 02, 2017.

[10] K. Georgilas, R. H. U. Khan, and M. E. Kartal, "The influence of pulsed laser powder bed fusion process parameters on inconel 718 material properties," *MATERIALS SCIENCE AND ENGINEERING A-STRUCTURAL MATERIALS PROPERTIES MICROSTRUCTURE AND PROCESSING*, vol. 769, JAN 2 2020.

[11] P. Zhou, Z. Liu, X. Xu, and X. Chu, "Comparative study on the propagation performance of coherently combined and incoherently combined beams," *OPTICS COMMUNICATIONS*, vol. 282, pp. 1640–1647, APR 15 2009.

[12] Y. Li, L. Qian, D. Lu, D. Fan, and S. Wen, "Coherent and incoherent combining of fiber array with hexagonal ring distribution," *OPTICS AND LASER TECHNOLOGY*, vol. 39, pp. 957–963, JUL 2007.

[13] H. Fathi, M. NÃ¤rhi, and R. Gumenyuk, "Towards ultimate high-power scaling: Coherent beam combining of fiber lasers," *Photonics*, vol. 8, no. 12, 2021.

[14] T. Fan and A. Sanchez, "Coherent (phased array) and wavelength (spectral) beam combining compared," in *Fiber Lasers II: Technology, Systems, and Applications* (L. Durvasula, A. Brown, and J. Nilsson, eds.), vol. 5709 of *PROCEEDINGS OF THE SOCIETY OF PHOTO-OPTICAL INSTRUMENTATION ENGINEERS (SPIE)*, pp. 157–164, SPIE; Southampton Photon Inc, 2005. Conference on Fiber Lasers II, San Jose, CA, JAN 24-27, 2005.

[15] J. R. Leger, "External methods of phase locking and coherent beam addition of diode lasers," in *Surface Emitting Semiconductor Lasers and Arrays*, pp. 379–433, Academic, Boston, 1993.

[16] M. Ito and T. Kimura, "Temperature stabilization in semiconductor laser diodes," *IEEE Journal of Quantum Electronics*, vol. 17, no. 5, pp. 796–798, 1981.

[17] J. Svarny, "Thermal stabilizer for laser diode," in *2006 International Conference on Applied Electronics*, pp. 205–208, 2006.

[18] S. Kaim, "Effects of forced airflow cooling on laser beam heating of volume bragg gratings," *Excerpt from the Proceedings of the 2013 COMSOL Conference in Boston*, 2013.

[19] D. Drachenberg, I. Divliansky, V. Smirnov, G. Venus, and L. Glebov, "High power spectral beam combining of fiber lasers with ultra high spectral density by thermal tuning of volume bragg gratings," in *FIBER LASERS VIII: TECHNOLOGY, SYSTEMS, AND APPLICATIONS* (J. Dawson and E. Honea, eds.), vol. 7914 of *Proceedings of SPIE*, SPIE; NKT Photon A/S; Fianium Ltd; PolarOnyx Inc, 2011. Conference on Fiber Lasers VIII - Technology, Systems, and Applications, San Francisco, CA, JAN 24-27, 2011.

[20] I. Divliansky, D. Ott, B. Anderson, R. Drachenberg, V. Rotar, G. Venus, and L. Glebov, "Multiplexed volume bragg gratings for spectral beam combining of high power fiber lasers," vol. 8237, 07 2013.

[21] Y. Han, W. Hao, Y. Dong, D. He, H. Cao, F. Kong, Y. Jin, and J. Shao, "High-efficiency, low-crosstalk multiplexed volume bragg grating for non-mechanical angular magnification," *Optics Laser Technology*, vol. 158, p. 108885, 2023.